Check for updates

The Meteoritical Society

Meteoritics & Planetary Science 58, Nr 6, 855–874 (2023)
doi: 10.1111/maps.13998

Al Huwaysah 010: The most reduced brachinite, so far

Cristian CARLI[1]*, Anna BARBARO[2,3], Mara MURRI[2,4], Maria Chiara DOMENEGHETTI[2], Antonio LANGONE[5], Enrico BRUSCHINI[1], Alice STEPHANT[1], Matteo ALVARO[2], Stefania STEFANI[1], Tiberio CUPPONE[6], Martina CASALINI[6], Alessandra MIGLIORINI[1], Ted L. ROUSH[7], and Giovanni PRATESI[6]

[1]IAPS-INAF, Rome, Italy
[2]Department of Earth and Environmental Sciences, University of Pavia, Pavia, Italy
[3]Department of Geoscience, University of Padua, Padua, Italy
[4]Department of Earth Science and Environmental Sciences, University of Bicocca-Milano, Milan, Italy
[5]IGG-CNR, Pavia, Italy
[6]Department of Earth Science, University of Firenze, Firenze, Italy
[7]Astrobiology and Space Sciences Division, Planetary Systems Branch, NASA Ames Research Center, Mountain View, California, USA
*Corresponding author.
Cristian Carli, IAPS-INAF, Rome, Italy.
E-mail: cristian.carli@inaf.it

(Received 28 September 2022; revision accepted 04 May 2023)

Abstract–Al Huwaysah 010 is an ungrouped achondrite meteorite, recently referred to as a brachinite-like meteorite. This meteorite, showing a fine-grained assemblage of low-Ca pyroxene and opaque phases, is strongly reduced in comparison to other reduced brachinites. The occurrence of some tiny plates of graphite and oldhamite in this meteorite suggests that a partial melt residue has experienced a further reduction process. Olivine, the most abundant phase, is compositionally homogeneous ($Fo_{83.3}$) as well as the clinopyroxene ($En_{45.5}Fs_{10.8}Wo_{43.7}$) and the plagioclase ($Ab_{69.5}$). Orthopyroxene ($En_{85.4}Fs_{13.9}Wo_{0.7}$) also occurs but only in a fine intergrowth. Other accessory phases are Fe metal grains (Ni-free or Cr-bearing Fe-Ni alloy), troilite, chlorapatite, pentlandite (as inclusions in chromite). The sample shows two different closure temperatures: the highest (≈900°C) is determined via the olivine–chromite intercrystalline geothermometer and the lowest temperature (≈520°C) is determined via the pyroxene-based intracrystalline geothermometer. These temperatures may represent, respectively, the closure temperature associated with the formation and a subsequent impact event excavating the sample from the parental body. The visible to near-infrared (VNIR) reflectance spectra of Al Huwaysah 010 exhibit low reflectance, consistent with the presence of darkening components, and weak absorptions indicative of olivine and pyroxene. Comparing the spectral parameters of Al Huwaysah 010 to potential parent bodies characterized by olivine–pyroxene mineralogy, we find that it falls within the field previously attributed to the SIII type asteroids. These results lead us to classify the Al Huwaysah 010 meteorite as the most reduced brachinite, whose VNIR spectral features show strong affinities with those of SIII asteroids.

INTRODUCTION

Achondrites are usually classified according to their similarities in isotopic composition, whole-rock chemistry, petrographic features, and mineral chemistry (Grady et al., 2014). This enables the affiliation of samples probably coming from similar parent bodies to a unique meteorite group. However, a portion of the achondrites remains ungrouped. They represent the products of material that experienced variable levels of

© 2023 The Authors. *Meteoritics & Planetary Science* published by Wiley Periodicals LLC on behalf of The Meteoritical Society.
This is an open access article under the terms of the Creative Commons Attribution License, which permits use, distribution and reproduction in any medium, provided the original work is properly cited.

differentiation and they presumably come from different bodies with respect to those ascribed to the existing meteorite groups of achondrites (Mittlefehldt, 2014; Greenwood et al., 2017).

Among the achondritic meteorites, those with the highest amount of olivine are brachinites. They can be considered peridotitic meteorites whose composition varies from dunitic to wehrlitic. In fact, it has been suggested that the group experienced a formation under conditions of relatively slow cooling (Keil, 2014). In this group, according to Keil (2014), the most abundant phase is represented by olivine (ol 71–96 vol%) together with variable amounts of clinopyroxene (cpx <15 vol%), plagioclase (plg 0–10 vol%), and orthopyroxene (opx 0–20 vol%). Other phases, such as Fe-sulfides (0–7 vol%), chromite (0–5 vol%), phosphates (0–3 vol%), and metallic Fe-Ni (0–2 vol%), always occur in lower amounts. Considering that brachinites are the products of igneous processes, their mineral compositions are homogeneous within each individual meteorite although, between different meteorites, the compositional range can also be quite wide. For example, the multiple analyses undertaken over time on different brachinites gave the following compositional ranges (Keil, 2014): ol ~$Fo_{64–73}$; cpx ~$En_{43–63}Wo_{36–48}$; plg ~$An_{15–33}$; opx ~$En_{69–73}Wo_{2–4}$.

As for the detailed processes of the petrogenesis of brachinites, there is currently no overall consensus among the scientific community. Even the petrofabric seems to show differences if distinct meteorites are considered (Hasegawa et al., 2019) implying that the parent body(s) of the brachinite group of meteorites experienced diverse igneous processes. Nevertheless, the group of brachinites is still poorly constrained. Brachinites are currently constrained by different characteristics, such as petrology, mineralogy, whole-rock chemical composition, and oxygen isotopic composition (Crossley et al., 2020; Day et al., 2012, 2019; Goodrich et al., 2011, 2017; Greenwood et al., 2007, 2012; Hasegawa et al., 2019; Rumble III et al., 2008), but several meteorites show similar characteristics with some deviation, for example, olivine and oxygen isotopic compositions or textures (e.g., Crossley et al., 2020; Day et al., 2019; Goodrich et al., 2017; Hasegawa et al., 2019).

Considering that different meteorites have been classified as brachinites, brachinite-like achondrites, or assigned to ungrouped achondrites with affinity to brachinites, and some achondrites are defined as brachinites even if no detailed studies are present (e.g., Crossley et al., 2020; Day et al., 2012; Goodrich et al., 2017; Hasegawa et al., 2019). For this reason often in the literature, the term clan has been used, to consider all of these meteorites together. It has even highlighted that within the brachinite group, the most classical brachinites are derived from a precursor that was more oxidized and sulfur-rich than those associated with the brachinite-like achondrites (e.g., Crossley et al., 2020). This apparent redox trend is associated with silicate FeO content and Fe/Mn ratios which, as suggested, may be used as a proxy for determining the relative oxidation state within brachinite group (e.g., Crossley et al., 2020; Goodrich et al., 2017). For this reason, it has been suggested to reclassify the brachinite group into a continuum of oxidized to reduced endmembers (e.g., Crossley et al., 2020).

This is why a detailed study of the ungrouped achondrites can be extremely useful in ascertaining if they do, or do not, belong to the brachinite group of meteorites.

Among ungrouped achondrites that deserve detailed study is Al Huwaysah 010. It is a find consisting of two fragments (total mass of 1411.79 g), collected in Oman on January 2, 2010 (Ruzicka et al., 2015). Both fragments lack a fusion crust and are reddish brown. Al Huwaysah 010 was classified as a weakly shocked (S2) ungrouped achondrite related to the brachinites and in particular similar to the ungrouped achondrites NWA 1500 and NWA 4042 (Ruzicka et al., 2015). Indeed, Crossley et al. (2020) stated that it appears to be more similar to NWA 4042, although it also shares a few of the characteristics identified in NWA 1500 (Goodrich et al., 2011). Nevertheless, Ruzicka et al. (2015) and Crossley et al. (2020) were unable to clearly define the nature of the relationships between Al Huwaysah 010 and the brachinites or brachinite-like meteorites. However, even if Al Huwaysah 010 shows similar oxygen isotope values of the brachinites ($\delta^{17}O = 2.31‰$, $\delta^{18}O = 4.73‰$, and $\Delta^{17}O = -0.15‰$, Greenwood et al., 2017), the composition of some mineral phases is different when compared with the same phases occurring in the brachinites (Day et al., 2012; Grady et al., 2014; Greenwood et al., 2017; Mittlefehldt et al., 2003).

Here, we describe the results of a multidisciplinary effort to characterize the chemical, mineralogical, and spectral properties of Al Huwaysah 010 meteorite with the aim to (i) provide more insights into the evolutionary history of this ungrouped achondrite and (ii) assess potential parent bodies via comparison of spectral reflectance features. We report results obtained by multiple techniques that included: scanning electron microscopy (SEM), electron probe microanalysis (EPMA), visible and near-infrared (VNIR) reflectance spectroscopy, single crystal X-ray diffraction (SC-XRD), micro-Raman spectroscopy (MRS) and laser-ablation inductively coupled-plasma mass spectrometry (LA-ICP-MS).

SAMPLES AND METHODS

Two samples of Al Huwaysah 010 were kindly loaned for this study by the Natural History Museum in Bern (Switzerland). A 1-inch circular polished thin section

19455100, 2023, 6, Downloaded from https://onlinelibrary.wiley.com/doi/10.1111/maps.13998 by Universita Di Firenze Sistema, Wiley Online Library on [10/08/2023]. See the Terms and Conditions (https://onlinelibrary.wiley.com/terms-and-conditions) on Wiley Online Library for rules of use; OA articles are governed by the applicable Creative Commons License

(hereafter PTS, size of the sample 20 × 15 mm) and a 2.23-g cut piece (subsequently CP, about 21 × 8 × 5 mm in size) were selected from the interior of Al Huwaysah 010 (n. 1001-010), reducing the impact of terrestrial alteration with respect to other pieces of this meteorite. We carried out optical and electron microscopy together with microprobe analyses on both thin section and the cut piece (Figure S1) in order to investigate the petrography and the mineralogical assemblage, and to apply the olivine–chromite intercrystalline geothermometer (e.g., Wlotzka, 2005) using EPMA. A small portion of the sample (0.15 gr.), representative of the bulk, has been crushed, to separate single crystals of clinopyroxene and to produce a powder for reflectance spectroscopy. In addition, XRD and EPMA analyses obtained from two single-crystal clinopyroxenes allowed us to obtain the closure temperature of the Fe-Mg exchange reaction (e.g., Alvaro et al., 2015; Domeneghetti et al., 2013; Murri et al., 2016, 2018, 2019). To perform the LA-ICP-MS, a small piece, taken from the CP sample, was embedded into epoxy (referred to subsequently as E-CP). Thus, a further electron microscopy study was performed on the E-CP to exactly locate the suitable areas for LA-ICP-MS analyses. Trace elements were measured on olivine and clinopyroxene single crystals in order to compare their compositions with those obtained from the same minerals in other achondrites. Reflectance spectroscopy measurements were performed on the CP and on a small amount of powder material in order to find a possible match of reflectance spectra with others in spectral virtual libraries (e.g., RELAB, https://pds-speclib.rsl.wustl.edu/).

Here, we provide a summary of the methods used in this study, more detailed information can be found in the supplementary online material.

Optical Microscopy

Observations of the PTS in transmitted (both planar and crossed polar) and reflected light were performed using a Zeiss Axioplan II optical microscope equipped with a Zeiss Axiocam camera (see Figure S2).

SEM and Energy-Dispersive X-Ray Spectroscopy

Three different SEMs, all equipped with energy-dispersive x-ray spectroscopy (EDS), were used.

a. The low vacuum SEM, FEI Quanta 200, was mainly used for the first characterization of the surface of the CP sample.
b. The E-CP, previously embedded in epoxy and carbon coated, has been analyzed in order to locate the phases and the areas suitable for the LA-ICP-MS analysis.
c. The Zeiss EVO MA15 was used for detailed recognition and identification of the phases in the PTS.

Modal Analysis

Two different survey scales (macroscale and microscale) were used for the modal analysis in order to optimize the accuracy of the data obtained.

For the macroscale investigation, we acquired 245 backscattered (BSE) images (with the corresponding elemental maps) at 100× magnification in order to cover as large an area as possible of the polished surface section. This global analysis has the advantage of providing a more statistically significant estimate of the phase abundance as it investigates a larger area at a lower magnification.

We selected 17 areas to acquire higher resolution (500× magnification) BSE images to take account of the small grain size of some phases. We also acquired the relative Ca and Si X-ray elemental maps, in order to discriminate plagioclase and clinopyroxene between the silicate phases during the process of the modal analysis. The images are 16-bit gray scale and are 2048 × 1536 pixels.

The analysis was done by thresholding the different gray scale values with a specific software producing five different layers corresponding to: (1) holes or phases with low BSE signal; (2) low-Ca pyroxene; (3) olivine; (4) high-Ca pyroxene; (5) opaque phases or phases with high BSE signal (see online material for more details).

Electron Probe Microanalysis

Quantitative mineral analyses of the main phases were performed on PTS using a JEOL JXA-8230 Super Probe equipped with five wavelength-dispersive spectrometers (WDS). All data were then processed with the iteratively corrective ZAF data reduction model (see online material for more details).

SC-XRD and EPMA on Pyroxene Single Crystals

SC-XRD analysis was performed on clinopyroxene crystals to calculate the closure temperatures of the intracrystalline Fe-Mg exchange reaction using the geothermometric calibration obtained by Murri et al. (2016). Two clinopyroxene crystals (50 × 40 × 10 μm) were extracted from the crushed portion of the CP sample with the aid of a sharp needle and their quality was checked by optical microscopy (for the absence of twinning) and by SC-XRD (for sharp peak profile). The SC-XRD analyses report the unit cell parameters, the discrepancy indices R_{merge}, R_{all}, R_w on all the Fo^2 and the goodness of fit (S) of the structure refinements for the two crystals (see Table S4).

19455100, 2023, 6, Downloaded from https://onlinelibrary.wiley.com/doi/10.1111/maps.13998 by Universita Di Firenze Sistema, Wiley Online Library on [10/08/2023]. See the Terms and Conditions (https://onlinelibrary.wiley.com/terms-and-conditions) on Wiley Online Library for rules of use; OA articles are governed by the applicable Creative Commons License

The two clinopyroxene crystals used for the SC-XRD analyses were embedded in epoxy and polished for EPMA analysis. After the polishing procedure, only one crystal was suitable for the chemical analysis. Major and minor elements, including halogens, have been determined by means of JEOL 8200 Super Probe—operating in X-ray wavelength-dispersive mode (WDS-EPMA).

Micro-Raman spectroscopy

The MRS analysis was performed on the oldhamite crystals occurring on the surface of an E-CP sample of Al Huwaysah 010 meteorite. The E-CP sample was polished to abrade the superficial weathering and the samples were maintained in a humidity-controlled condition until the Raman measurement. The MRS analysis was performed using a Horiba LabRam HR Evolution spectrometer equipped with an Olympus BX41 confocal microscope at the controlled temperature of 20 (±1) °C.

Laser Ablation Inductively Coupled Plasma Mass Spectrometry

The laser probe employed in this study has a fundamental emission in the infrared at 1064 nm. For this work, the laser was operated at a repetition rate of 10 Hz, and the spot diameter was 50 μm with a pulse energy of about 0.1 mJ.

Reproducibility and accuracy of the REE concentration values were assessed on the reference sample BCR2-g. The precision of the BCR2-g measurements is reported as percent relative standard deviation (%RSD) for each element, which is calculated as the standard deviation divided by the average concentration. The %RSD provides an estimate of the consistency of the analyses of the BCR2-g, and so the reproducibility of the measurement. The accuracy is generally high (<15%) for all the elements except for Cr (−34%) and Zn (−29%).

VNIR Reflectance Spectroscopy

The reflectance spectroscopy measurements were performed, at room temperature and pressure in the VNIR for both powder and sample surfaces (hereafter called slab) from the CP. From the crushed portion of the sample, we prepared a dry sieved powder at <100 μm for reflectance measurements. After the first set of VNIR measurements, we performed a rust removal procedure (Kiddel et al., 2018) to document the possible influence of the weathering products on the spectral features.

The VNIR range (0.35–2.5 μm) was investigated with a relatively large spot (6 mm) but acquiring spectra in different points on the slab surface. Multiple acquisitions were also obtained for the powder sample, and spectra were averaged, to avoid sample preparation error (see also Carli et al., 2018).

RESULTS

Petrography

As illustrated in Figure 1, the sample has a protogranular texture (Figure S2). Each of the main phases, olivine, Ca-rich pyroxene, plagioclase, and chromite, shows a homogeneous grain size distribution. In general, the crystal size of the main silicates falls within the range of 200–300 μm. A few crystals of these phases can be larger; some elongated olivine crystals may reach 600 μm whereas the larger Ca-pyroxene and plagioclase grains can reach 800 and 1600 μm, respectively. Only a few triple junctions are visible with optical microscopy because the ragged texture of the sample makes their identification very difficult; conversely, when BSE images are used, the triple junctions can be seen more easily thanks to the polygonal network of secondary opaque phases (Figure 1).

The modal mineralogy analysis yields different results depending on whether it is calculated at the macroscale or at the microscale. This is due to the fine intergrowth of Ca-poor orthopyroxene with weathered opaque phases occurring at the border and inside olivine crystals, as shown in Figure 2.

At the macroscale (lower magnification), the modal values are similar to those observed in the brachinites and brachinite-like meteorites (Keil, 2014): olivine accounts for 78.5 vol% of the sample, Ca-rich pyroxene for 5.7 vol %, plagioclase for 3.0 vol%, chromite for 2.0 vol%, accessory phases (Ni-free iron, troilite, graphite, and Ni-rich iron sulfide) for 1.0 vol%, and weathering phases represent 9.8 vol%. The low-Ca pyroxene at the lower used magnification cannot be discriminated due to its fine crystal size. The weathering products are mainly iron oxides and oxyhydroxides, Ca-sulfates, and Ca-Mg carbonates. No hydrated silicate phases were detected.

At the microscale (higher magnification), when the details of the intergrowth can be resolved and the phases automatically recognized (Figure 2), the modal percentage of olivine and low-Ca pyroxene, calculated from the 17 BSE images, yields a mean value of 64.4 and 12.1 vol%, respectively. The different results obtained at the microscale are mainly due to the difficulty in discriminating between olivine and the assemblage of low-Ca pyroxene plus metal (and the weathering products) during the image analysis at the macroscale. As a consequence, even the modal percentage of weathering phases (12.8 vol%) is higher with respect to that calculated at the macroscale, and the greater weathering vol% is mainly attributable to oxidized metals. The

19455100, 2023, 6, Downloaded from https://onlinelibrary.wiley.com/doi/10.1111/maps.13998 by Universita Di Firenze Sistema, Wiley Online Library on [10/08/2023]. See the Terms and Conditions (https://onlinelibrary.wiley.com/terms-and-conditions) on Wiley Online Library for rules of use; OA articles are governed by the applicable Creative Commons License

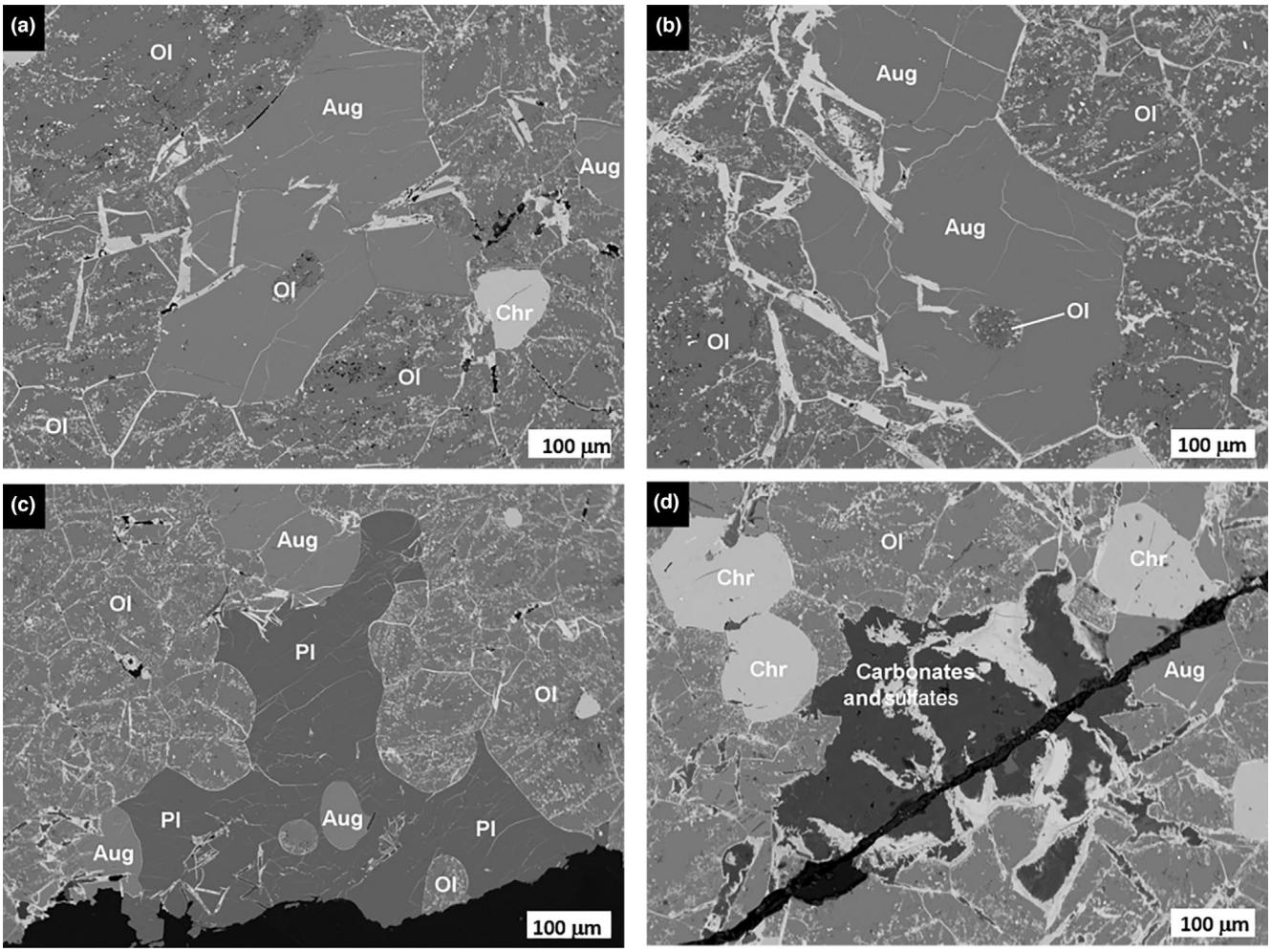

FIGURE 1. Backscattered electron (BSE) images of Al Huwaysah 010 (CP sample). (a, b) Large grain of poikilitic high-Ca pyroxene (Aug) containing rounded olivine (Ol) chadacrysts; it is interesting to note that the appearance of olivine grains is clearly affected by the same fine intergrowth of low-Ca pyroxene and dendritic opaque phases characterizing all the olivines in the sample. In the images, laths of iron oxide and grains of chromite are also visible (lighter gray). (c) Rounded grains of high-Ca pyroxene poikilitically enclosed in a large grain of plagioclase (Pl). (d) Olivine crysts characterized by a fine intergrowth of low-Ca pyroxene and dendritic opaque phases (Figure 2), rounded grains of high-Ca pyroxene, and crysts of chromite (chr) with the presence of an assemblage of carbonates and sulfates (terrestrial weathering).

percentages of Ca-rich pyroxene, plagioclase, chromite, and accessory phases remain unchanged.

Some thicker dendritic veins (up to 50 µm) developed both along the boundary of the silicate phases and across the olivine crystals where they appear to be always intermixed with low-Ca pyroxenes. We emphasize that neither high-Ca pyroxenes nor the plagioclases (Figure 1) are affected by the pervasive presence of the assemblage of dendritic iron oxides and low-Ca pyroxene.

In the investigated thin section, the formation of continuous Fe-rich thin veins (mainly composed of iron oxides and oxyhydroxides) can be associated with weathering products (Figure 3). These veins occur almost exclusively along the boundary of the silicate phases. Within these thin veins, we also observed the presence of Mg-Ca carbonates and Ca sulfate (Figure 1d). As previously reported in the study of Crossley et al. (2020), we observed that even the olivine has experienced weathering because some grains show the presence of iddingsite. Iron oxyhydroxides (Figure 3a,c) accompany or represent further branches of oxide dendritic veins. Conversely, in all the samples, we did not observe distinguishable alteration associated with primary metal grains.

Mineralogy

The textural appearance of the abundant olivine is ragged (Figure 3b,d), due to the presence of a fine-grained assemblage of low-Ca pyroxene and dendritic opaque

19455100, 2023, 6, Downloaded from https://onlinelibrary.wiley.com/doi/10.1111/maps.13998 by Universita Di Firenze Sistema, Wiley Online Library on [10/08/2023]. See the Terms and Conditions (https://onlinelibrary.wiley.com/terms-and-conditions) on Wiley Online Library for rules of use; OA articles are governed by the applicable Creative Commons License

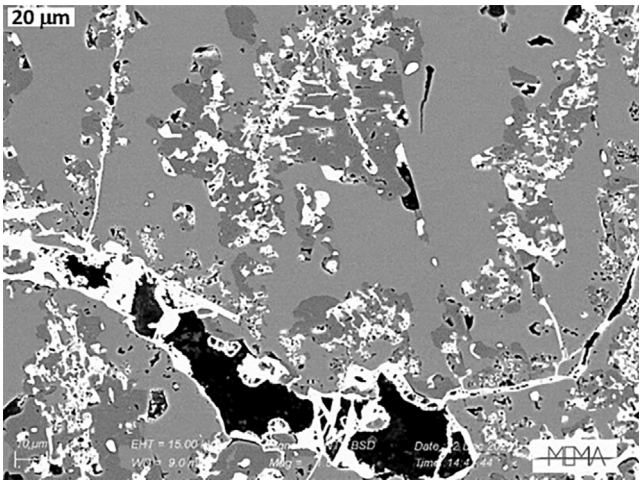

FIGURE 2. BSE high magnification image of the Al Huwaysah 010 showing that all olivine crystals (light gray) contain diffuse very fine-grained aggregates of orthopyroxene (gray) + Fe metal and its weathering products (white).

phases which line the boundaries of the olivine crystals and penetrate them. We noted also that such a fine-grained assemblage is present in the rounded grains of olivine chadacrysts poikilitically enclosed in the high-Ca pyroxene (Figure 1a), similar to what has been reported for NWA 7605 (Irving et al., 2013). Olivine, compositionally homogeneous (Table 1) and devoid of any normal or reverse zonation (Table S1), is characterized by a high amount of magnesium ($Fo_{83.3}$) and a low (29.3) Fe/Mn molar ratio.

In contrast to olivine, high-Ca pyroxene grains, occurring as subhedral or anhedral augite ($En_{45.5}Fs_{10.8}Wo_{43.7}$ and mg# 80.2, see Table 1), are never affected by the pervasive presence of the fine-grained assemblage of opaque phases (weathered metal and sulfides) and low-Ca pyroxene, even when they are poikilitically enclosed in plagioclase (Figure 1b).

This fine intergrowth is probably not ubiquitous in the Al Huwaysah 010 specimen considering that it was not detected by Crossley et al. (2020). This fine intergrowth represents the only mode of occurrence of the low-Ca pyroxene, whose composition ($En_{85.4}Fs_{13.9}Wo_{0.7}$ and mg# 85.6, see Table 1) shows a lower iron content compared to augite. Both pyroxenes are compositionally homogeneous and no compositional zonation was observed. Plagioclase feldspar occurs both as allotriomorphic or large poikilitic anhedral grains which may enclose small round high-Ca pyroxene grains (Figure 1b). Quantitative compositional analyses performed on plagioclase consistently yielded a composition $Ab_{69.5}$ (Table 1).

The chromite, like the other phases, is homogeneously distributed in the sample as euhedral or subhedral grains whose compositions correspond to chromite ($Cr/Cr + Al = 0.795$; $Fe/Fe + Mg = 0.634$). The accessory phases are represented by granular chlorapatite, small grains of iron, tens of microns long, that are notably Ni-free iron and Cr-bearing Fe-Ni alloy, a few microns wide plates of graphite (Figure S3), troilite, and pentlandite (as inclusion in chromite).

Iron oxides, iron oxyhydroxides, calcium sulfate (anhydrite), and dolomite are also present, probably formed due to the terrestrial weathering that affected Al Huwaysah 010. A Raman spectrum collected from the surface of the E-CP sample, inside of an anhydrite grain, shows the presence of oldhamite (Figure S4).

Trace Element

Several grains of olivine were analyzed for trace element contents. A significant portion of the acquired data is affected by spikes, especially of Ni, due to the presence of small inclusions of Fe-Ni metal that severely compromised the results. Only five analyses were selected as the most representative of olivine free of inclusions (Table S2). Sc, Ti, V, Cr, Mn, Co, Ni, Cu, Zn, Sr and Y were detected for olivine; only a few of them provided RSD lower than 20% (Sc and Mn; Figure 4); the other elements show a larger variability among different grains with RSD in the range of 20%–40% (Ti, V, Zn, and Y) or even higher (Cr, Co, Ni, Sr). Olivine shows high concentrations of Mn, in the range of 3501–3908 ppm (average 3678 ± 162 ppm). Cr, Co, and Ni vary considerably from a few ppm up to hundreds ppm (Table S2), whereas Ti and V are in the range of about 16–38 and 19–37 ppm, respectively. Lower concentrations were obtained for Sc (4–7 ppm) and Zn (2–5 ppm); Cu Sr and Y are lower than 2 ppm.

Clinopyroxene was analyzed several times but due to small inclusions only five analyses were considered as representative. For several elements, the precision was better than 10% (Na, Al, Sc, Ti, V, Cr, Mn, Sr), while Co, Zn, Y, and Ho provided RSD in the range of 12%–16% whereas the other elements show a major scatter with RSD up to 53%. Clinopyroxene contains thousands of ppm of Na, Al, Cr, and Mn; Ti and V range between 658 and 717 ppm and 331 and 366 ppm, respectively. Sc, Co, Ni, and Zn show average values of 79, 37, 104, and 72 ppm, respectively; B ranges from about 6 to 11 ppm whereas Sr and Y have average values of 5 and 2 ppm, respectively. Cu, Zr, and the rare earth elements are generally below 1 ppm. The REE-normalized pattern for Al Huwaysah 010 is characterized by a fractionation of middle- and heavy-REE that are fairly flat with CI-like abundances whereas the light-REE are depleted relative to CI abundances (Figure 5, Table S3).

19455100, 2023, 6, Downloaded from https://onlinelibrary.wiley.com/doi/10.1111/maps.13998 by Universita Di Firenze Sistema, Wiley Online Library on [10/08/2023]. See the Terms and Conditions (https://onlinelibrary.wiley.com/terms-and-conditions) on Wiley Online Library for rules of use; OA articles are governed by the applicable Creative Commons License

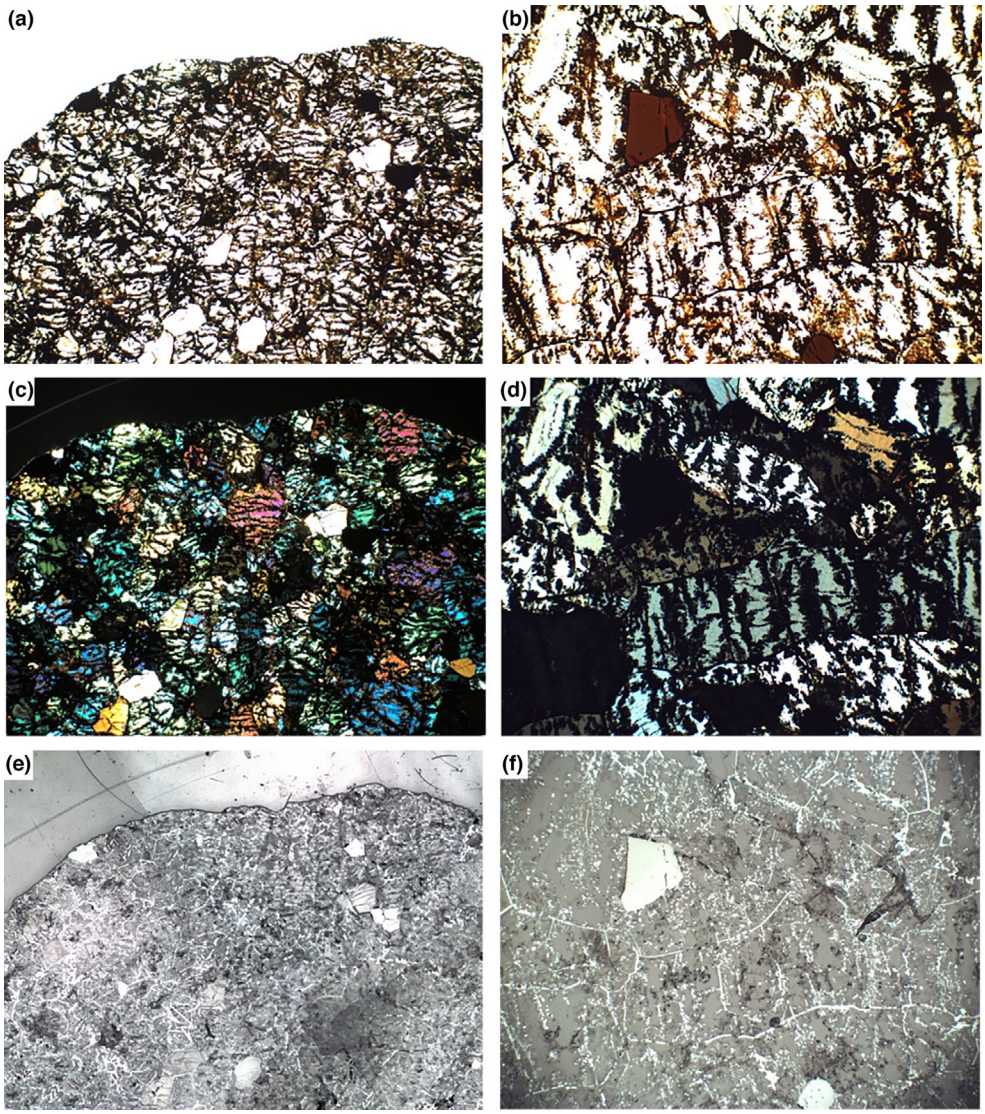

FIGURE 3. Optical microscopy images of PTS sample of Al Huwaysah 010. Two different areas of the sample, at two different magnifications (left column: field of view 5.2 × 3.9 mm; right column: field of view 1.4 × 1.0 mm), are represented. From top to bottom: (a, b) transmitted plane polarized light (PPL) images showing a network of opaque phases (iron oxides), readily visible as thin black veins, and yellow-brown veins (iron oxyhydroxides); (c, d) transmitted cross polarized light (XPL) images showing the ragged edges and fracture, sawtooth texture, of olivine; (e, f) reflected light images showing several spinels (lighter gray) along with the network of iron oxides and oxyhydroxides (dark gray). (Color figure can be viewed at wileyonlinelibrary.com)

Geothermometry

Olivine–Chromite Geothermometer

The olivine/Cr-spinel and olivine/chromite thermometers are substantially based on Fe-Mg partitioning between olivine and Cr-spinel/chromite (Calafiore, 2002; Johnson & Prinz, 1991; Sack & Ghiorso, 1991a; Wlotzka, 1985).

The Al Huwaysah 010 meteorite is characterized by a homogeneous composition of olivine and chromite; therefore, the mean composition has been used here for our calculations since Kessel et al. (2007) demonstrated that temperature calculated on the average composition is very similar to the average temperature calculated from a group of temperatures obtained from the individual olivine–spinel pairs. Data on the chemical composition of olivine and chromite are those obtained during this study by means of EPMA (Table 1).

The closure temperature for the olivine–spinel system was calculated using MELTS online tool based on the thermodynamic models and numerical calculation developed by Sack and Ghiorso (1991a, 1991b). This

19455100, 2023, 6, Downloaded from https://onlinelibrary.wiley.com/doi/10.1111/maps.13998 by Universita Di Firenze Sistema, Wiley Online Library on [10/08/2023]. See the Terms and Conditions (https://onlinelibrary.wiley.com/terms-and-conditions) on Wiley Online Library for rules of use; OA articles are governed by the applicable Creative Commons License

TABLE 1. Average compositions of the major phases in the Al Huwaysah 010 meteorite.

	Olivine	High-Ca pyroxene	Low-Ca pyroxene	Plagioclase	Spinels
Number of data	18	18	13	8	8
SiO_2	40.32	54.58	57.55	61.07	n.d.
TiO_2	0.02	0.13	0.02	0.03	1.07
Al_2O_3	0.01	0.72	0.01	24.16	9.76
Cr_2O_3	0.03	0.68	0.08	n.d.	56.79
FeO	15.56	7.08	9.97	0.09	22.65
MnO	0.51	0.20	0.53	n.d.	0.46
MgO	45.13	16.06	32.99	0.03	7.43
CaO	0.06	20.99	0.39	6.08	0.02
Na_2O	n.d.	0.35	0.01	7.79	n.d.
K_2O	n.d.	n.d.	n.d.	0.1	n.d.
NiO	0.01	0.01	0.01	n.d.	n.d.
V_2O_3	0.01	0.05	0.01	n.d.	0.73
ZnO	0.02	0.02	0.03	0.01	0.04
Total	101.65	100.87	101.58	99.30	98.97
Fo	83.3				
Range	82.7–83.9				
Fe/Mn	29.4				
Fs		10.8	13.9		
Range		10.27–11.99	13.28–15.40		
En		45.5	85.4		
Range		45.24–46.25	83.89–85.80		
Wo		43.7	0.7		
Range		42.11–44.36	0.58–0.89		
Ab				69.5	
Range				67.67–70.34	
Fe/Fe + Mg					0.634
Range					0.63–0.64
Cr/Cr + Al					0.795
Range					0.79–0.80

Note: Data in wt%. All the measured spots are in Table S1. For oxides, n.d., not detected.

procedure yielded a closure temperature of 941 ± 37°C. Using the same model, the calculation of the oxygen fugacity from the olivine–spinel–orthopyroxene equilibrium (Sack & Ghiorso, 1989, 1994a, 1994b, 1994c) provides a value of log fO_2 IW-1.7 at a pressure of 0.1 kbar.

Another useful model for calculating the closure temperature of the olivine–spinel system is that based on the equation developed by Wlotzka (2005). The temperatures derived from this equation differs from those derived from Fabriès (1979), mainly at low Cr/(Cr + Al) ratios, because the Fabriès (1979) temperatures increase with decreasing Cr/(Cr + Al) ratio, whereas the modified version of Wlotzka (2005) yields constant temperatures throughout. The closure temperature obtained with Wlotzka (2005) model is 864 ± 42°C. The differences of closure temperature values from the two models are common as discussed by Wlotzka (2005). In our case, the results suggest a closure temperature near ~900°C.

Closure Temperature of Mg-Fe Reaction of Clinopyroxenes

The results of EPMA performed on the Al Huwaysah 010_3 clinopyroxene single crystal after XRD analysis are reported in Table S5. In the same table, the sum of the mean atomic numbers (m.a.n.) at M1 and M2 sites (34.26 electrons per formula unit, e.p.f.u.) calculated from the analysis is also reported. This value is in very good agreement with the sum of the m.a.n.s of M1 + M21 + M21 sites obtained from the structure refinement before introducing the chemical constraints for sample 3 (34.28) and within 2σ for sample 1.

All of the selected clinopyroxenes have Fs contents (with $Fs = 100 \times \Sigma Fe/[\Sigma fe + Mg + Ca]$ where $\Sigma fe = Fe^{2+}Fe^{3+}Mn$) within the compositional range of Fs_9 to Fs_{24} (Murri et al., 2016).

The Fe^{2+}-Mg ordering state was obtained from the site populations to calculate the closure temperature by means of the intracrystalline distribution coefficient (kD), using Equation (1):

19455100, 2023, 6, Downloaded from https://onlinelibrary.wiley.com/doi/10.1111/maps.13998 by Universita Di Firenze Sistema, Wiley Online Library on [10/08/2023]. See the Terms and Conditions (https://onlinelibrary.wiley.com/terms-and-conditions) on Wiley Online Library for rules of use; OA articles are governed by the applicable Creative Commons License

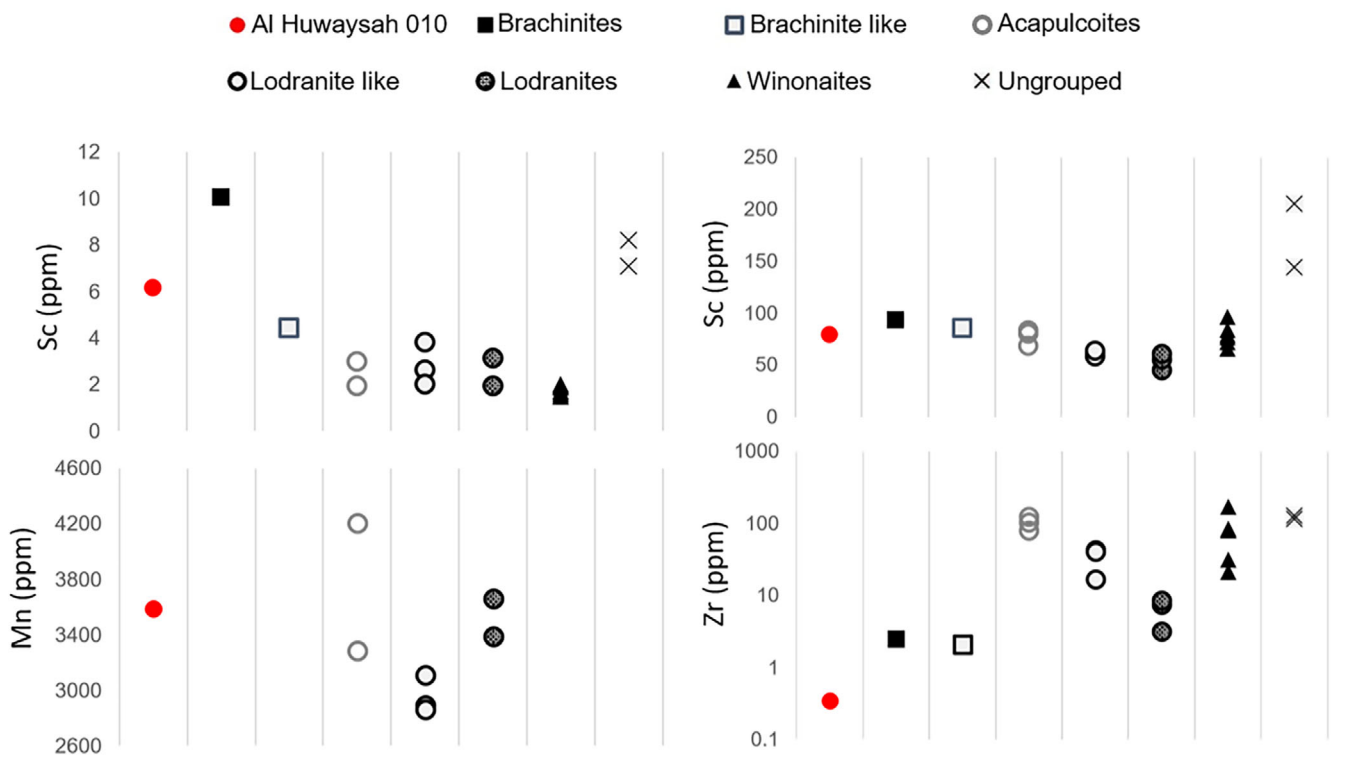

FIGURE 4. Trace elements in olivine (on the left) and clinopyroxene (on the right) measured by LA-ICP-MS. In particular, here it is possible to observe the Sc and Mn values for olivine (ppm), and the Sc, Zr of Al Huwaysah 010 compared to brachinite EET 99402 and brachinite-like NWA 5400 (Mn in ol not determined for NWA 5400; Day et al., 2012); acapulcoites (Acap.) Acapulco and ALHA 81261 (Floss, 2000); anomalous lodranites (An) ALHA 81187, ETT84302, and GRA 95209 (Floss, 2000); lodranites MAC 88177 and LEW 88280 (Floss, 2000); winonaite (Win) NWA 1463, Pontlyfni, Winona, Mt. Morris, Tierra Blanca (Floss et al., 2008); HAH 193 (Floss et al., 2007, 2008); and ungrouped meteorites GRA 06128 and GRA 06129 (Day et al., 2012). (Color figure can be viewed at wileyonlinelibrary.com)

$$kD = \left[\left(Fe^{2+}\ M1\right)\ (MgM2)/\left(Fe^{2+}\ M2\right)(MgM1)\right]. \quad (1)$$

The relationship between the distribution coefficient (kD) and T_C is usually expressed using calibration equations of the ln(kD) as a function of $1/T(K)$. The site populations obtained from the structural refinements with chemical constraints and the distribution coefficients (kD) with relative propagated errors are reported in Table S6.

For these samples, the calibration equation by Murri et al. (2016), given as Equation (2) here, was used because it produces reliable results on clinopyroxene samples with compositions ranging between Fs_9 and Fs_{24} as demonstrated from the investigation on synthetic samples (Murri et al., 2018). In particular, the equation was obtained using data by Murri et al. (2016) on an augite from Theo's Flow (TS7 N.16, Fs_9) together with those by Alvaro et al. (2015) on augites from the Miller Range nakhlite sample (MIL 03346, Fs_{24}).

$$\ln(kD) = -4040\ (\pm 180)/T(K) + 1.12\ (\pm 0.17)\ \left(R^2 = 0.988\right). \quad (2)$$

The calculated T_C for the two crystals of Al Huwaysah 010 are 529 ± 30°C and 514 ± 27°C, respectively. Therefore, the average intracrystalline closure temperature for Al Huwaysah 010 is 520 ± 30°C.

REFLECTANCE SPECTROSCOPY

Spectral reflectance is generally acquired on powders, thus reducing the number of measurable meteorites and limiting the study of their heterogeneity. In this study, the analysis was performed on both a slab and a powder, allowing spectral properties to be obtained for both sample types. The slab sample was also measured after the rust removal procedure (see "VNIR Reflectance Spectroscopy" Section). The information derived from spectral analysis is

19455100, 2023, 6, Downloaded from https://onlinelibrary.wiley.com/doi/10.1111/maps.13998 by Universita Di Firenze Sistema, Wiley Online Library on [10/08/2023]. See the Terms and Conditions (https://onlinelibrary.wiley.com/terms-and-conditions) on Wiley Online Library for rules of use; OA articles are governed by the applicable Creative Commons License

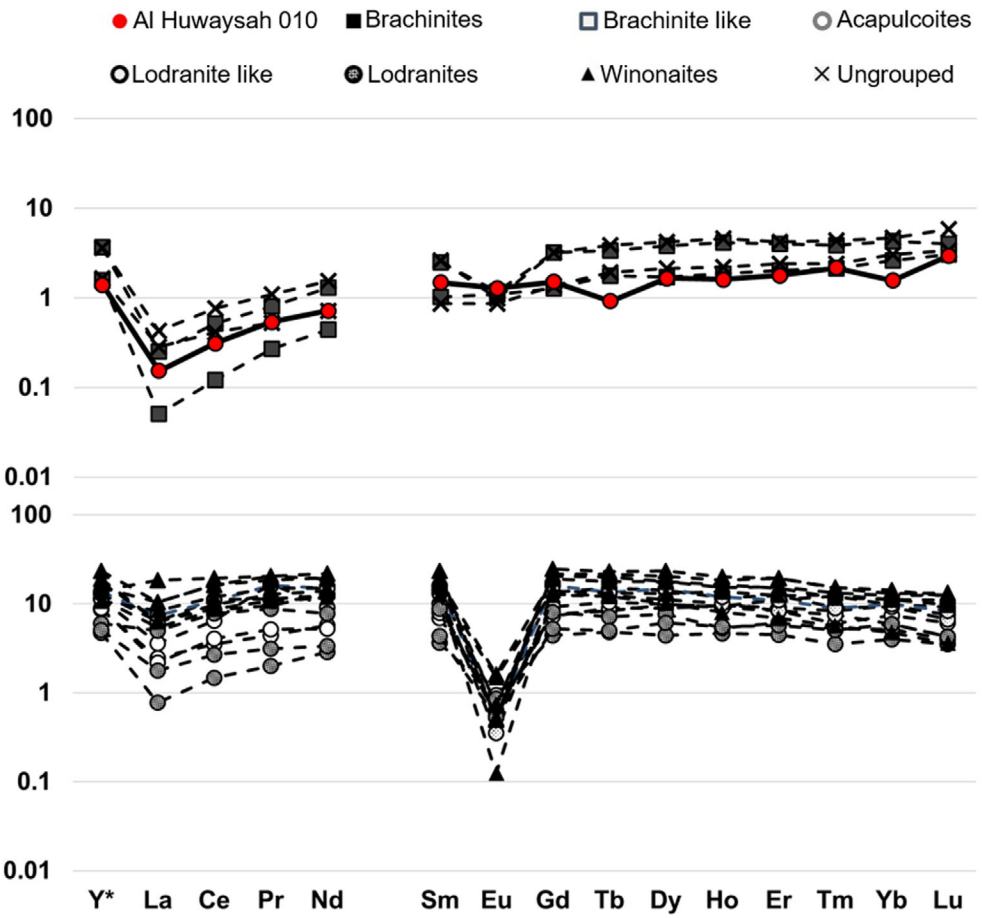

FIGURE 5. Trace elements in clinopyroxene measured by LA-ICP-MS. It is possible to observe the REE patterns for clinopyroxenes of Al Huwaysah 010 compared to brachinite EET 99402 and brachinite-like NWA 5400, and two ungrouped meteorites GRA 06128 and GRA 06129 acapulcoite-related in the top panel. In the lower panel, we report also data for the primitive achondrites (Acap) Acapulco and ALHA 81261; anomalous lodranites (An) ALHA 81187, ETT84302, and GRA 95209; lodranites MAC 88177 and LEW 88280; winonaites (Win) NWA 1463, Pontlyfni, Winona, Mt. Morris, Tierra Blanca, HAH193. From these plots, it is clear that Al Huwaysah 010 shows the lower Eu anomaly with respect to the other considered achondrites. (Color figure can be viewed at wileyonlinelibrary.com)

strengthened by the identification of mineral chemistry and sample texture investigations.

The use of VNIR spectral ranges allowed us to characterize the mineralogy from the VNIR spectra often used for comparison with properties of their potential parent bodies (i.e., asteroids) and other meteorite groups. Moreover, this procedure defines the detection limits and our capability to retrieve mineralogical information for planetary bodies.

The VNIR reflectance spectra of the powder and slab are presented in Figure 6. It shows the meteorite spectra have: (i) low reflectance, probably due to the fine-grained crystal sizes of the minerals and the particular textures within dark veins of fine intergrowth of low-Ca pyroxene and dendritic opaque phase, and also the presence of minor carbon phases and metals; (ii) two major bands at about 1 and 2 μm (red arrows) that are commonly associated with Fe^{2+} in crystalline sites of pyroxenes and olivine (1 μm): the green arrow indicates the possible effect of olivine, at wavelength longer than the pyroxenes band center (BC) at around 1 μm (e.g., Burns, 1993), (iii) two minor and weak absorptions, indicated by the blue arrows and more evident in the continuum removed plot (Figure S9), are probably related to charge transfer, or spin-forbidden Fe transitions, in silicates (e.g., Burns, 1993); (iv) lack of obvious M-OH (M can include Fe, Al, and Mg cations) due to hydroxylated materials and H_2O absorptions, near 1.4–1.5 and 1.9 μm, respectively (see Clark, 1999), despite the evidence of weathering. The measurements acquired after the rust treatment (Figure S9) show the same properties summarized above but a reduced intensity of the charge transfer absorptions and a shift of the two major bands to lower wavelengths.

19455100, 2023, 6, Downloaded from https://onlinelibrary.wiley.com/doi/10.1111/maps.13998 by Universita Di Firenze Sistema, Wiley Online Library on [10/08/2023]. See the Terms and Conditions (https://onlinelibrary.wiley.com/terms-and-conditions) on Wiley Online Library for rules of use; OA articles are governed by the applicable Creative Commons License

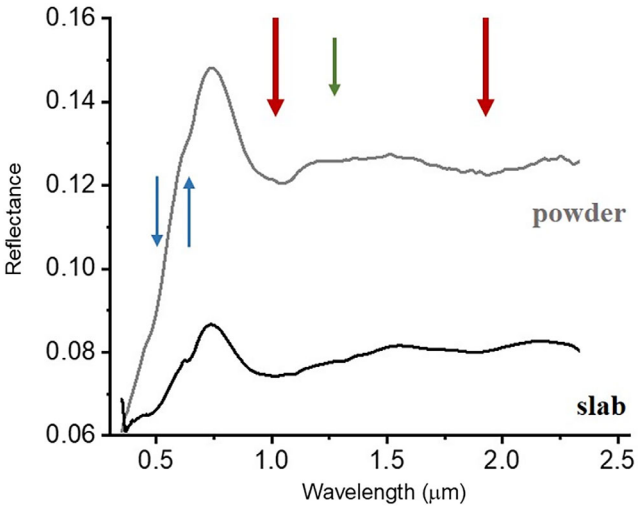

FIGURE 6. Reflectance spectra of Al Huwaysah in the VNIR for the powdered sample, <100 μm (gray) and an average of six different points in the slab (black). Spectra are smoothed with FFT of 20 points for powder and 50 points for slab in the NIR (>1 μm); moreover, they are truncated after 2.4 μm, since at longer wavelengths, measured reflectance was highly variable. The arrows indicate spectral features discussed in the text. (Color figure can be viewed at wileyonlinelibrary.com)

The continuum line is calculated as straight-line segments, as a function of wavelength, that join the reflectance maxima in the spectrum (Clark & Roush, 1984) and the main spectral parameters were calculated from the continuum removed spectra. To compare assemblages of olivine and pyroxene: (1) The BC is calculated as the position of the minimum reflectance of the band after the continuum removal. To avoid any effects due to noise, we fitted the minimum region with a second-order polynomial; (2) the band area ratio (B.A.R.) is calculated as the integrated area between the continuum and the spectra once the continuum is removed (see Carli et al., 2022 and reference therein).

DISCUSSION

The existence of ungrouped meteorites often reflects our difficulty in placing these specimens in a correct interpretative framework. The issue is not only taxonomic but also genetic. The problem is even more relevant when it concerns achondrites. These meteorites experienced a series of very complex processes ranging from partial differentiation to complete fusion.

In particular, there has recently been a debate about the issues surrounding the classification of brachinites and brachinite-like meteorites. First of all, the question arises as to the purpose of the meteorite classifications, that is, whether it is useful simply as a means of schematizing acquired knowledge or whether it is a fundamental means of achieving a genetic and/or evolutionary interpretation. While the latter appears to be the most convincing answer, it should be noted that—from a strictly genetic point of view—it is often difficult to determine whether meteorites belong to the same parent body or to different parent bodies.

The literature on brachinites and brachinite-like meteorites often deals with this question providing different but not definitive answers (Crossley et al., 2020; Day et al., 2012, 2019; Goodrich et al., 2011, 2017; Greenwood et al., 2007, 2012; Hasegawa et al., 2019; Rumble III et al., 2008).

Petrography, Mineralogy, and Mineral Chemistry: A Comparison with Other Brachinite and Brachinite-Like Meteorites

Due to the presence of a fine-grained mineralogical assemblage, the observed modal mineralogy of Al Huwaysah 010 is highly dependent on the magnification used to obtain the images on which to calculate it. At lower magnification, the values of olivine and Ca-rich clinopyroxene (78.5 and 5.7 vol%, respectively) are in the range observed for other brachinites and brachinite-like meteorites, where olivine is always the major phase (>68 and up to 96 vol%) and the Ca-rich pyroxene ranges from 3.6 to 15 vol% (Crossley et al., 2020; Day et al., 2012; Goodrich et al., 2011, 2017). On the other hand, at higher magnification, the olivine content is much lower (64.4 vol%) whereas the low-Ca orthopyroxene and the weathering products are higher (12.1 and 12.8 vol% respectively). The amounts observed at higher magnification are certainly more reliable and reflect the strong in situ reduction experienced by this meteorite. The amount of other phases not involved in the reduction process, like high-Ca clinopyroxene (5.7 vol%), plagioclase (3.0 vol%), chromite (2 vol%), remains unchanged whether low or high magnification is employed. Sulfides, metal, and phosphates also occur in lower amounts in brachinites/brachinite-like meteorites (Day et al., 2012), although sulfides and metal can be readily observed when the meteorites have not experienced significant weathering.

The mineralogical assemblage occurring in Al Huwaysah 010 is a widespread fine-grained assemblage where opaque phases are associated with Ca-poor orthopyroxene. This texture is similar to that observed in Divnoe, NWA 6112, MIL 090206, MIL 090304, MIL 090405, and other brachinite/brachinite-like meteorites, where opaque phases occurring in the fine-grained assemblage along with orthopyroxene are mainly represented by Fe-sulfide and Fe-Ni metal (Goodrich et al., 2011, 2017; Hasegawa et al., 2019; Irving et al., 2013; Rumble III et al., 2008). Moreover, in Al

19455100, 2023, 6, Downloaded from https://onlinelibrary.wiley.com/doi/10.1111/maps.13998 by Universita Di Firenze Sistema, Wiley Online Library on [10/08/2023]. See the Terms and Conditions (https://onlinelibrary.wiley.com/terms-and-conditions) on Wiley Online Library for rules of use; OA articles are governed by the applicable Creative Commons License

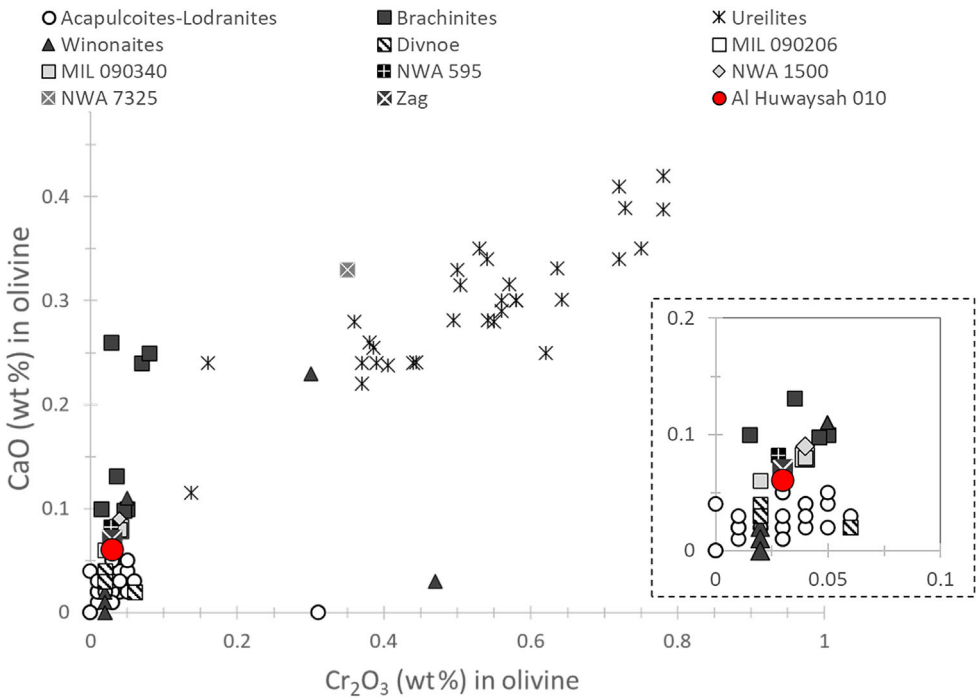

FIGURE 7. CaO versus Cr_2O_3 in olivine of some achondrite groups. Modified after Goodrich et al. (2011). The plot shows how Al Huwaysah 010 is close to Zag and it lies between the acapulcoites–lodranites and brachinites, which as a similar Cr_2O_3 range and different CaO. (Color figure can be viewed at wileyonlinelibrary.com)

Huwaysah 010, almost all olivine–olivine, olivine–augite, and olivine–chromite grain boundaries are lined with such fine-grained assemblages and they also occur as patches within olivine (Figure 2) and even in olivine chadacrysts enclosed in Ca-rich clinopyroxene (Figure 1b). The assemblage of iron oxides and low-Ca pyroxenes (Figures 1 and 2) crosscutting the olivine crystals could resemble the sawtooth texture of some ureilites (Figure S5). However, in ureilites, such a texture is related to the occurrence of "reduction rims" in olivine grains due to a reaction with graphite-generating metal via smelting, that is, reduction of oxidized iron in silicates (Goodrich, 1992; Mittlefehldt et al., 1998; Wlotzka, 1972). Evidence of such reduction rims has been observed in NWA 1500 by Goodrich et al. (2011) and a slight reverse chemical zoning ($Fo_{72–74}$) has also been detected in MIL 090206, MIL 090304, MIL 090405 meteorites. In the Al Huwaysah 010 portion studied here, we did not find such rims nor they have been reported for this meteorite by other authors (Crossley et al., 2020; Ruzicka et al., 2015). It is worth mentioning, however, that such rims could have been erased by a heating event or by the high degree of terrestrial weathering experienced by Al Huwaysah 010.

When the composition of silicate minerals is considered, differences and analogies between Al Huwaysah 010 and the brachinites (or brachinite-like meteorites) can be found. Olivine in Al Huwaysah 010 (Table 1) has a higher amount of Mg ($Fo_{83.3}$) compared to all the known brachinites, where the composition usually ranges from Fo_{64} to Fo_{70}. These differences, however, become less pronounced when specific brachinites (or brachinite-like achondrites) are considered where olivine ranges from Fo_{72} to Fo_{80} (Crossley et al., 2020; Goodrich et al., 2011; Greenwood et al., 2017; Hasegawa et al., 2019; Irving et al., 2013). A clear difference may also be observed between the value of molar Fe/Mn (29.4) in olivine of Al Huwaysah 010 and those of other brachinites (52–77). Nevertheless, even in this case, the gap decreases if the values of some specific meteorites (e.g., NWA 6112) are considered.

In spite of the different content of Fo, plotting CaO versus Cr_2O_3 of the Al Huwaysah 010 overlies some brachinite-like meteorites that fall close to the low CaO limit field of brachinites (Figure 7). Al Huwaysah 010 plots well separated from ureilites and at slightly higher CaO values with respect to acapulcoites and lodranites that remain consistent with where Divnoe plots.

Pyroxene compositions of Al Huwaysah 010 (Table S1) are much more similar to those of brachinites: indeed, augite ($Fs_{11.6}Wo_{42.8}$) is in the same range reported by Keil (2014) for high-Ca pyroxene in brachinites

19455100, 2023, 6, Downloaded from https://onlinelibrary.wiley.com/doi/10.1111/maps.13998 by Universita Di Firenze Sistema, Wiley Online Library on [10/08/2023]. See the Terms and Conditions (https://onlinelibrary.wiley.com/terms-and-conditions) on Wiley Online Library for rules of use; OA articles are governed by the applicable Creative Commons License

($Fs_{9\text{-}14}Wo_{38\text{-}48}$); regarding the low-Ca pyroxene, Al Huwaysah 010 has an iron content slightly lower ($Fs_{15.0}Wo_{0.7}$) than the values reported by Goodrich et al. (2011) for brachinites ($Fs_{17\text{-}30}Wo_{1\text{-}4}$; Figure S6).

When plots of Al_2O_3, Cr_2O_3, TiO_2 versus Mg# are considered, the contents of these elements in augite of Al Huwaysah 010 fall completely inside the field of brachinites (or brachinite-like) meteorites (Figure S7; Goodrich et al., 2011).

The plagioclase ($An_{29.95}$) of Al Huwaysah 010 shows a Ca abundance that is in the range of the compositions reported by Goodrich et al. (2011) for the brachinites or the brachinite-like meteorites ($An_{22\text{-}41}$).

As for spinel composition (Figure S8), both the molar Cr/(Cr + Al) and Fe/(Fe + Mg) values are consistent with those of chromites reported for other brachinites and brachinite-like achondrites (Gardner-Vandy et al., 2013; Johnson et al., 1977; Mittlefehldt et al., 2003; Nehru et al., 1983; Warren & Kallemeyn, 1989). Furthermore, their TiO_2 and V_2O_3 contents are similar to those of most brachinites and brachinite-like achondrites but higher than those of chromites in ureilites, winonaites, and many acapulcoites and lodranites.

Some considerations can also be made with regard to the trace elements in silicate minerals, as measured by LA-ICP-MS. In particular, olivine in Al Huwaysah 010 (Figure 4 and Tables S2 and S3) has Sc (6 ppm), Ti (29 ppm), V (30 ppm), and Y (0.07 ppm) contents within the range of EET 99402, GRA 06128, GRA 06129, and NWA 5400 (Day et al., 2012). Conversely, U content is higher, but its concentration may be affected by the weathering process of the desert environment. As for high-Ca clinopyroxene, Y and Zr appear to be particularly distinctive compared to other achondrite groups (Figure 8). In Al Huwaysah 010 Y content appears to be distinct from acapulcoites, lodranites and winonaites and similar to that of the brachinite EET 99402, two ungrouped achondrites and the brachinite-like NWA 5400. Whereas the Zr content although different from other achondrites, it is similar to EET 99402 and NWA 5400, and very different from the two ungrouped achondrites. Noteworthy, unlike other elements, Al-Kathiri et al. (2005) suggested Zr in the meteorites from Oman have been affected to a very small extent (i.e., slightly depleted) by weathering.

However, the high-Ca clinopyroxene REE pattern is one of the most interesting features in providing a valuable comparison among the achondrite groups. In the pattern of Al Huwaysah 010, and those of other brachinites and brachinite-like achondrites (Day et al., 2012), LREE have low abundances (<1 CI-chondrite), with HREE > LREE (La/Yb = 0.14). Furthermore, the LREE and HREE (Figure 5) of Al Huwaysah 010, EET 99402, GRA 06128, GRA 06129,

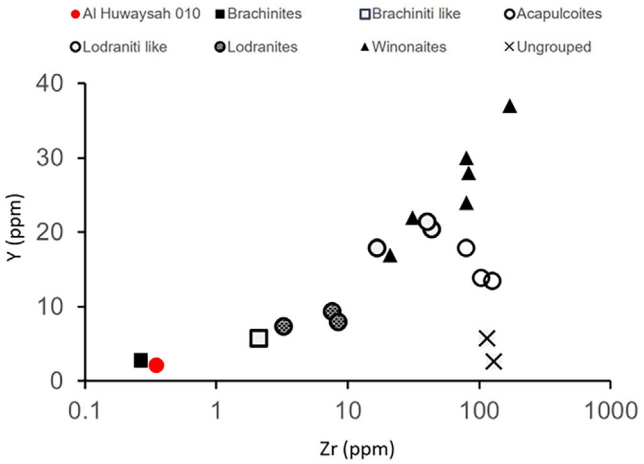

FIGURE 8. Comparison of the ppm of Y and Zr in Al Huwaysah 010 clinopyroxene with those in primitive achondrites (brachinite EET 99402 and brachinite-like NWA 5400); acapulcoites (Acap) Acapulco and ALHA 81261; anomalous lodranites (An) ALHA 81187, ETT84302, and GRA 95209; lodranites MAC 88177 and LEW 88280; winonaites (Win) NWA 1463, Pontlyfni, Winona, Mt. Morris, Tierra Blanca, HAH193; and ungrouped meteorites GRA 06128 and GRA 06129 measured by LA-ICP-MS. Al Huwaysah 010 is similar only to the brachinite EET 99402 (see the main text for references). (Color figure can be viewed at wileyonlinelibrary.com)

NWA 5400 appear to show the strongest depletion compared to acapulcoites, lodranites, and winonaites (Day et al., 2012). Regardless of the abundances, while LREEs have a very similar pattern in all groups, HREEs show a diversified pattern compared to brachinites (or brachinite-like) which show a very small or barely noticeable negative Eu anomaly.

The most recent and reliable oxygen isotope data (Greenwood et al., 2017) clearly show that Al Huwaysah 010 plots in the same area as the brachinites. Some brachinite-like meteorites also plot in this area although other brachinite-like meteorites fall outside the brachinite field and sometimes overlap the Terrestrial Fractionation Line. The brachinite field is partially overlapped by HED, main group pallasite, and angrite meteorites (see figure 7 in Greenwood et al., 2017), but Al Huwaysah 010 is in a portion of the brachinite field not overlapped by other groups (see figure 19 in Greenwood et al., 2017). The oxygen isotope analysis of Al Huwaysah 010 plots close to those of Divnoe, NWA 6112, MIL 090206, MIL 090304, MIL 090405. These meteorites, along with other brachinites/brachinite-like meteorites, show a similar texture showing fine-grained assemblage where Fe-sulfide and Fe-Ni metal are associated with Ca-poor orthopyroxene (Goodrich et al., 2011, 2017; Hasegawa et al., 2019; Irving et al., 2013; Rumble III et al., 2008).

19455100, 2023, 6, Downloaded from https://onlinelibrary.wiley.com/doi/10.1111/maps.13998 by Universita Di Firenze Sistema, Wiley Online Library on [10/08/2023]. See the Terms and Conditions (https://onlinelibrary.wiley.com/terms-and-conditions) on Wiley Online Library for rules of use; OA articles are governed by the applicable Creative Commons License

Geothermometrical Interpretation and Comparison with Other Meteorites

Olivine–Chromite Geothermometry and Oxygen Fugacimetry

As presented in "Geothermometry" Section, Al Huwaysah 010 closure temperature values calculated with two intercrystalline olivine–chromite geothermometers show a value close to 900°C. These temperatures are in the range of those previously obtained for Divnoe (~830°C), NWA 6112 (~860°C), and MIL 090206 plus its pairs MIL 090340 and MIL 090405 (~910°C), which have been attributed to the brachinite group by Hasegawa et al. (2019). Moreover, the temperatures yielded by olivine–chromite geothermometry for Al Huwaysah 010 are also similar to those obtained in other studies of brachinites (e.g., Goodrich et al., 2017; Petaev & Brearley, 1994).

The calculated oxygen fugacity (IW-1.7) of Al Huwaysah 010 is in the range (IW-1.16 to IW-2.14) calculated by Crossley et al. (2020) for other brachinites.

CPX T_C Interpretation and Comparison with Other Meteorites Groups

The average closure temperature obtained from intracrystalline Mg-Fe exchange reaction in clinopyroxene is 520 ± 30°C. This value is lower by several hundreds of degrees compared to the temperatures obtained from the intercrystalline olivine–chromite geothermometers. The large deviation between these two temperatures could be mainly due to the fact that intracrystalline geothermometry relies on the cation exchange between crystallographic sites within a single crystals and not among two different mineral phases; thus, its sensitivity to temperature changes is higher and the exchange reaction can proceed to much lower temperatures with respect to the intercrystalline process. This could mean that (i) the recorded thermal event is the same as the one detected with intercrystalline geothermometry, just followed to much lower temperatures, or (ii) this low closure temperature has been reached after a subsequent thermal event (which reopened the system) with respect the one associated with the olivine–chromite derived temperatures. These results for two cpx crystals of Al Huwaysah 010 ungrouped meteorite were then compared with T_C literature data obtained on orthopyroxene samples from other achondrites (Zema et al., 1997) and cpx sample from Martian nakhlites (Domeneghetti et al., 2013). It is evident that Al Huwaysah 010 plots near the temperature range of primitive achondrites A-L (acapulcoites and lodranites).

Reflectance Spectra Comparison

The VNIR spectra of Al Huwaysah 010 were compared to all the achondrites (excluding the HEDs due to the clear spectral differences) from RELAB library to define relationships with the spectral shape (Figure 9).

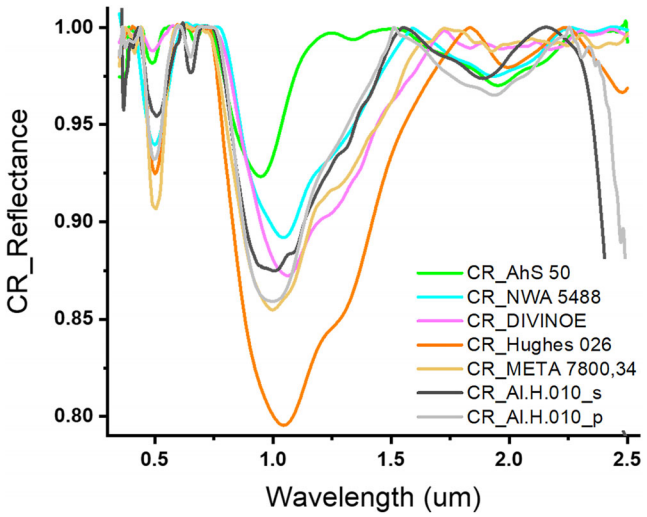

FIGURE 9. VNIR continuum removed spectra of Al Huwaysah 010 (black, slab, and gray, powder) compared with the most similar reflectance spectra of meteorites found in RELAB spectral library. The Huwaysah spectra here are smoothed with an FFT smoothing of 50 points to reduce the noise. (Color figure can be viewed at wileyonlinelibrary.com)

The results of mineral chemistry and mineral abundance permit us to highlight the information that can be retrieved from the reflectance spectroscopy. Here, we discuss those results with respect to other meteorites and meteorite groups and to potential parental bodies.

In Figure 9, we plot the VNIR continuum removed spectra of Al Huwaysah 010 slab and powder, comparing them with those from meteorites that show the best match. In particular, we have seen a match with a ureilite (META78008), a brachinite (Hughes 026), a lodranite (NWA 5488), an anomalous meteorite (Divnoe), and an anomalous polymict ureilite (Almahata Sitta 50, hereafter AhS 50). In detail, all these selected meteorites show absorption associated with olivine at 1 μm, except for AhS 50 where pyroxenes dominate this spectral region, and some of them, as well as Al Huwaysah 010, show an absorption at 2 μm band (very weak in Divnoe and META 78008, and absent in Hughes 026) which probably can be ascribed to pyroxenes. This second band is partially influenced by the combined presence of a weak 1.9 μm water absorption, which is clearly evident in Hughes 026.

In the visible range, some weak absorptions are also present which could be assigned to spin forbidden transitions due to Fe^{2+} in mafic minerals (Burns, 1993).

VNIR reflectance spectra clearly illustrate how Al Huwaysah 010 has a mineral assemblage mainly dominated by olivine with associated pyroxene.

Compared to other meteorites, we can see a similarity with other achondrites where olivine is the prevalent phase

19455100, 2023, 6, Downloaded from https://onlinelibrary.wiley.com/doi/10.1111/maps.13998 by Universita Di Firenze Sistema, Wiley Online Library on [10/08/2023]. See the Terms and Conditions (https://onlinelibrary.wiley.com/terms-and-conditions) on Wiley Online Library for rules of use; OA articles are governed by the applicable Creative Commons License

(Divnoe and Hughes 026) but at the same time, in the NIR, also with a spectrum that do not fit an olivine-dominated material (AhS 50). The 1 μm absorption centered at 998 or 1005 nm, for powder or slab, respectively, is consistent with the composition of the olivine ($Fa_{16.2}$). This BC is at lower wavelengths with respect to the other meteorites where olivine is slightly Fe-enriched, Hughes 026 ($Fa_{34.5}$, Grossman, 1998) and Divnoe (Fa_{20-28}, Petaev & Brearley, 1994). The Al Huwaysah 1 μm BC positions are very close to META 78008_34 (which has $Fa_{23.7}$, Takeda et al., 1989). NWA 5488 also shows a band position at a similar wavelength despite the lower iron content (Fa_{10}, Weisberg et al., 2009). AhS 50 is spectrally different, showing a predominance of pyroxenes with respect to olivine. However, for this piece of Almahata Sitta sample, no mineral abundances are reported in literature, and only the mineral chemistry information is present, indicating that other than olivine (Fa_{8-15} similar to the sample studied here), there are low Ca pyroxene and pigeonite rich in Mg (Zolensky et al., 2010 and references therein). The spectral differences suggest that the piece measured for the reflectance should be pyroxene enriched with respect to the olivine amount that generally are present in these ureilites. The 2 μm absorption, slightly affected by the presence of a water absorption ascribed to alteration, shows a position compatible with the Mg-rich pyroxene composition, and similar to NWA 5488 and AhS 50. Pyroxene assemblages are slightly different in the Al Huwaysah 010, NWA 5488, and AhS 50, but all of them are mainly Mg-rich compositions where probably the low Ca component is spectrally dominating.

No mafic absorption is present around 2 μm for META 78008_34, Divnoe and Hughes 026, where pyroxenes are generally reported with values lower than 10%, and generally with low Fs values, except for Divnoe ($Fs_{20-28}Wo_{0.5-2.5}$).

Since the main phases are olivine and pyroxene, we calculated and plotted the spectral parameters, band I centers (BIC) and B.A.R., of Al Huwaysah 010 in Figure 10a and compare them to other achondrites. In BIC versus B.A.R. plots, olivine-dominated (ol-rich) mixtures fall closer to a B.A.R. value of zero with BIC at longer wavelengths than pyroxene-dominated mixtures. It is clear from Figure 10a that the Al Huwaysah 010 B.A.R. lies closer to the ol-rich meteorites, and the BIC, at a shorter wavelength compared to ol-rich meteorites that is consistent with the presence of pyroxenes, highlighted also by the spectral shape at 1 μm. In particular, we can see that the achondrites considered here move from primitive achondrites which have the lower BIC and higher B.A.R. They have often an average olivine between 28 and 36, and a correspondent pyroxenes abundance of 29 (opx > cpx) to 37 (opx > cpx) for lodranite and acapulcoite, with for both primitive achondrites a pyroxene (px) to olivine (ol) ratio (px/ol calculated as px/px + ol) of 0.51, with mafic material showing an Mg# closer to 90 (e.g., see Lucas et al., 2019). Decreasing the B.A.R., samples plot into the main ureilites field reported in Lucas et al. (2019) defined from the data of Cloutis et al. (2010). The ureilites studied by Cloutis et al. (2010) show a large px/ol ratio, but apart from a few cases, they cluster into a specific area with a px/ol between 0.08 and 0.6. The composition of mafic minerals in these samples shows a larger variation that expand from Mg# >90 to circa Mg# 75. So the definition of these fields is affected by the variation of ol/px abundance but even by the variation of opx/cpx and the Mg# of mafic phases.

The Al Huwaysah 010 measurements plot at BIC slightly higher than the ureilite field which is consistent with the olivine-dominated samples at BIC closer to Meta 7800 that has a px/ol ratio of 0.1 and mafic mineral has an Mg# around 80, both similar to the Al Huwaysah 010.

All of these achondrites, along with the Al Huwaysah 010, here, plot below the ol-opx line (thick gray line) defined by Cloutis et al. (1986), whereas the other basaltic achondrites (e.g., HEDs) plot above this line.

This same plot has been used to discuss the spectral variation for S-Type and the ol-dominated (A-Type) asteroids (Gaffey et al., 1993). When we plot the Al Huwaysah 010 points on Gaffey et al. (1993) diagram (Figure 10b), we see that the powder point (p) is just outside, while the slab point (s) falls within the upper left part of the SIII field of Gaffey et al. (1993).

This subtype is in general defined as indicative of the presence of calcic pyroxene, in particular, the portion where Al Huwaysah 010 falls is associated with cases where Band II area is underestimated, since Ca- rich pyroxene shows a Band II with a shoulder at wavelength larger than 2.5 μm or with the fact that some of them have a very weak band II.

When we considered the comparison with the meteorite points, instead we saw that ureilites are partially superimposed on the SIII field; and, in particular, increasing the olivine abundance, as well as the Fa content, the ureilite moved from higher B.A.R. and low BIC to lower B.A.R. and high BIC (Figure 10b). Al Huwaysah 010 also has a low px/ol and the slab spectra still fall within the SIII type asteroids. This illustrates how spectral parameters present in the SIII field are compatible with meteorites that have an important abundance of olivine with Mg# > 90 and not just related to the presence of Ca-bearing cpx.

Recently, DeMeo et al. (2022) investigated the potential connection between meteorites and parental body types. They relied upon spectral reflectance comparison of normalized reflectance using a chi-squared

19455100, 2023, 6, Downloaded from https://onlinelibrary.wiley.com/doi/10.1111/maps.13998 by Universita Di Firenze Sistema, Wiley Online Library on [10/08/2023]. See the Terms and Conditions (https://onlinelibrary.wiley.com/terms-and-conditions) on Wiley Online Library for rules of use; OA articles are governed by the applicable Creative Commons License

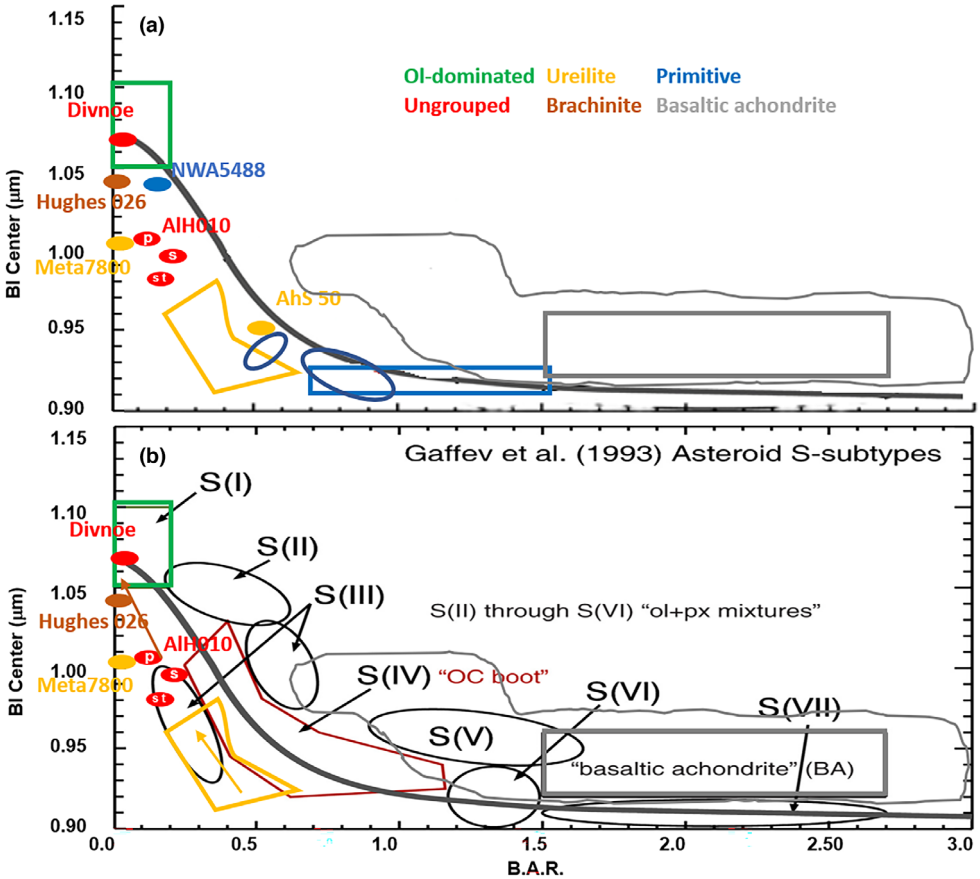

FIGURE 10. (a) Relationship between the BIC position and the B.A.R. modified after Lucas et al. (2019). Basaltic achondrite (dark gray rectangle), primitive achondrite, and ureilite fields are reported from Lucas et al. (2019, see their paper for further details). Light gray area which enlarged the basaltic achondrite field is after Carli et al. (2022). Ungrouped Divnoe, primitive NWA 5488, brachinite Hughes 026, ureilite Meta 78008, AhS 50 are from Relab library, and spectral indices are calculated as for Al Huwaysah 010 (AlH010 in the plot). p and s indicate spectra acquired on powder and on slab samples, respectively, and s_t indicates the spectra acquired on the slab after rust removal treatment. (b) Relationship between the BIC position and the B.A.R. modified after Gaffey et al. (1993) including the boxes related to S-type asteroids. Al Huwaysah 010 shows a relationship compatible with a portion of SIII-type asteroids, and it is just at lower BIC and higher B.A.R. with respect to the more common brachinites which show an olivine with higher iron abundance (the brown arrow shows the possible trend). This is similar to what can be seen for the ureilites which move (yellow arrow) from higher px/ol ratio and lower Mg# to sample with lower px/ol and higher Mg#, see data from Cloutis et al. (2010). (Color figure can be viewed at wileyonlinelibrary.com)

method to define the match. These authors make a connection between brachinite and A-type spectra (or Sa type, asteroids types that are ol-dominated), with four of 11 brachinites matching the A-type spectra. This is in accordance with what we observe here, in fact Hughes 026 has spectral parameters compatible with ol-dominated bodies, but it has an olivine composition richer in iron and higher olivine abundance, 90%–93% (Gardner-Vandy et al., 2013), compared to the Al Huwaysah 010 sample studied here. Other brachinites that approach the type A asteroid spectra, like Brachina and Eagles Nest, have similar olivine compositions and abundances (see DeMeo et al., 2022). Taking these constraints into account, it seems likely that the spectral properties of brachinites would be shifted depending on ratio of px to ol and the composition of the ol. In particular, B.A.R. versus BIC show a shift from samples with slightly higher px/ol and lower Fa to those with higher ol abundance and Fa. This is similar to what can be seen within the ureilite group, but just shifted to higher BIC. This implies that for at least this portion of S-type asteroids, considering mixing of primitive achondrite and iron meteorite (Hiroi et al., 1993) is not necessary to fit their spectral properties. The trends shown by ureilites and brachinites (considering also brachinites-like and ungrouped with affinity to brachinites) could explain those spectral properties. Additionally, Al Huwaysah 010 can be considered as a link between this S-type asteroid spectra and some A-type asteroid spectra following the different spectral properties of brachinites. This trend is

19455100, 2023, 6, Downloaded from https://onlinelibrary.wiley.com/doi/10.1111/maps.13998 by Universita Di Firenze Sistema, Wiley Online Library on [10/08/2023]. See the Terms and Conditions (https://onlinelibrary.wiley.com/terms-and-conditions) on Wiley Online Library for rules of use; OA articles are governed by the applicable Creative Commons License

also related to the iron composition of the brachinites and so to the more reducing conditions associated with Al Huwaysah with respect to the rest of brachinites as discussed above.

IMPLICATIONS

Considering the oxygen isotope data, we can certainly say that Al Huwaysah 010 formed either on the same parent body or in an area of the solar nebula with the same oxygen reservoir, as the other brachinites. Taking into account evolutionary aspects, Al Huwaysah 010 is a meteorite showing many characteristics (e.g., petrography, modal mineralogy, geochemistry, and oxygen isotopes) similar to other brachinites, although it has olivine and orthopyroxene richer in Mg, and the lowest Fe/Mn and Fe/Mg ratios with respect to brachinites.

Are these data sufficient to attribute this meteorite to brachinite group? As far Al Huwaysah 010, we prefer speak explicitly of reduced brachinites. The use of this term recalls the existence of reduced and oxidized members in this group of meteorites, as already suggested by Crossley et al. (2020). The material from which the brachinites have been generated may have experienced varying degrees of melting to produce brachinites with a quite varied modal mineralogy and mineralogical composition. In this interpretative framework, the felsic albitic plagioclase-rich meteorites (e.g., GRA 06128/9) could have been produced by partial melting at temperatures between Fe, Ni sulfide melting (950–980°C) and the onset of basaltic melting (>1050°C; Shearer et al., 2010), so representing an evolved felsic crustal material from the brachinite parent body (Day et al., 2009). As suggested by Day et al. (2012, 2019), partial melting may lead to the formation of residues that are increasingly magnesium-rich with increased extents of partial melting. This trend was also confirmed by Feldstein et al. (2001) who observed increasing Fo contents in restite olivine after prolonged disequilibrium melt experiments on the Leedey L6 chondrite.

Therefore, following Day et al. (2019) and Crossley et al. (2020), the brachinites group may represent a continuum from oxidized to reduced endmembers where the range of Fe/Mg observed is consistent with variable degrees of sodic, and high Fe/Mg melt extraction. This process could have been followed by prolonged equilibration at relatively medium–high temperatures, in their respective parent body(ies).

In this context, Al Huwaysah 010, that shows evidence of being the most reduced brachinite encountered to date, could represent a residue, characterized by Fo-enriched olivine, resulting from partial melting at temperature >900°C followed by an equilibration at lower temperatures (down to 520°C, as recorded by the intracrystalline Mg-Fe exchange reaction in clinopyroxene).

Nevertheless, in the parent body of Al Huwaysah 010, other processes could have occurred. Graphite, only reported in NWA 1500 and Ramlat as Sahmah 309 of the brachinite group of meteorites (Keil, 2014), still occurring (although in very small amount) throughout the investigated specimen, may have played an important role in the evolution process, since it may have acted as a trigger agent for the reduction reaction $Mg_2SiO_4 + Fe_2SiO_4 + C = 2(MgSiO_3) + 2Fe + CO_2$ yielding to the low-Ca orthopyroxene and opaque phases assemblage visible in the sample analyzed here. Alternative reduction process has also been suggested to include $Fe_2SiO_4 + CO \rightarrow FeSiO_3 + Fe + CO_2$ (Delaney et al., 2000) or methane infiltration and reaction with primary olivine $4(Fe\ Mg)SiO_4 + CH_4 = 4Fe + 4MgSiO_3 + CO_2 + 2H_2O$ (Irving et al., 2013). In such reactions, the amounts of metallic iron produced and the Fe/Mg ratios in both reactant olivine and product orthopyroxene could be variable.

Another interesting process is that suggested by Goodrich et al. (2011, 2017). For subpopulations of brachinites and ungrouped achondrites containing textures like those observed in Al Huwaysah 010 reduction of olivine to orthopyroxene and metals/sulfides through reaction with S-rich gas or fluids, namely, $Fa + Fo + S_2\ (g) \leftrightarrow En + FeS + O_2\ (g)$ has been suggested (Goodrich et al., 2011, 2017). The occurrence of S-rich gas or fluids may well have occurred also in Al Huwaysah 010, where a strong reduced phase like oldhamite has been detected.

The reflectance spectral properties of Al Huwaysah 010 show that this sample is far from olivine-dominated spectra even if the spectral parameters indicate that olivine is the main contributor. In fact, the comparison with other meteorites shows that the olivine abundance and its composition is dominating the spectral properties. Moreover, the position in the BIC and the B.A.R. values indicates that Al Huwaysah 010 is characterized by lower olivine amount and, in particular, lower Fa content among the brachinite group (Figure 10). This is similar to the trend seen also for the ureilites. Additionally, the spectral parameters of this sample plot within the SIII type asteroid field even if Ca-rich pyroxene is not the main phase implying that this spectral type could be described by spectral properties related to brachinite. In particular to brachinite samples with lower Fa and olivine, making, at least for some of them, a connection between some SIII type and A-Type asteroids, since comparing with other brachinite material, we can see that spectral properties move from Al Huwaysah 010 to Hughes 026, as well as others like Brachina and Eagles Nest, increasing the iron composition and/or olivine abundance. Examples of asteroids that plot closer to Al

19455100, 2023, 6, Downloaded from https://onlinelibrary.wiley.com/doi/10.1111/maps.13998 by Universita Di Firenze Sistema, Wiley Online Library on [10/08/2023]. See the Terms and Conditions (https://onlinelibrary.wiley.com/terms-and-conditions) on Wiley Online Library for rules of use; OA articles are governed by the applicable Creative Commons License

Huwaysah 010 are Eunomia, Ariadne, and Herculina (Gaffey et al., 1993) as well as Didymos (De Leon et al., 2006; 1996GT in their paper).

CONCLUSION

Al Huwaysah 010 shows evidence that correlates with brachinites (e.g., oxygen isotopes, see Greenwood et al., 2017, trace elements of olivine and clinopyroxenes, and minor elements on clinopyroxenes).

Conversely, mafic minerals have higher magnesian compositions with respect to other brachinites. Moreover, we found the presence of reduced phases like graphite and oldhamite associated with a particular texture with a fine-grained assemblage of low-Ca pyroxene and opaque phases.

These results indicate that Al Huwaysah 010 is the most reduced brachinite recognized so far. The oxygen isotopes of this meteorite overlap with those of the brachinite group, indicating that it formed in the same reservoir as the other brachinites. The enrichment in Mg of mafic minerals strongly suggests that this meteorite, similar to MIL 090206 (and the other paired MILs), represents a nearly pure residue after partial melting. The widespread fine-grained assemblage of low-Ca pyroxene and opaque phases was instead due to a further process of reduction related to the presence of C- and S-rich fluid (or gas). Just this last process is related to the occurrence of both graphite and oldhamite which have not previously been found together in the same meteorite.

Reflectance properties indicate the connection with the brachinites moving from sample with lower Fa (and px/ol ratio, like Al Huwaysah 010) to higher Fa composition. This is consistent with the fact that Al Huwaysah 010 could be a brachinite sample crystallized in more reducing conditions. Moreover, a comparison with the S-type asteroids shows a potential connection between the brachinite group and some objects of that asteroid group.

Acknowledgments—This manuscript is the first one published by Ol-BODIES (Olivine-Bearing ungrOuped achonDrites and their parent bodIES in the solar system) project thanks to the financial contribution from the agreement ASI-INAF n.2018-16-HH.0. This research utilizes spectra acquired by different investigators with the NASA RELAB facility at Brown university (Pieters & Hiroi, 2004); in Table S7 of the online material, we document the sample name and investigators. The authors thank the R.C. Greenwood, L. Pittarello and the editors, A. J. Timothy Jull, and, in particular, E. Cloutis, whose comments and suggestion permitted us to improve the quality of the paper.

Data Availability Statement—Data available on request from the authors.

Editorial Handling—Dr. Edward Anthony Cloutis

REFERENCES

Al-Kathiri, A., Hofmann, B. A., Jull, A. J. T., and Gnos, E. 2005. Weathering of Meteorites from Oman: Correlation of Chemical and Mineralogical Weathering Proxies with 14C Terrestrial Ages and the Influence of Soil Chemistry. *Meteoritics & Planetary Science* 40: 1215–39.

Alvaro, M., Domeneghetti, M. C., Fioretti, A. M., Cámara, F., and Marinangeli, L. 2015. A New Calibration to Determine the Closure Temperatures of Fe-Mg Ordering in Augite from Nakhlites. *Meteoritics & Planetary Science* 50: 499–507.

Burns, R. G. 1993. *Mineralogical Applications of Crystal Field Theory*, 2nd ed. New York, NY: Cambridge University Press. 523.

Calafiore, S. I. 2002. Implications of Olivine-Spinel Geothermometry for the Thermal Metamorphism of LL Chondrites. 33rd Lunar and Planetary Science Conference, abstract #1815.

Carli, C., Ciarniello, M., Migliorini, A., and Pratesi, G. 2022. Iron Rich Basaltic Eucrites, Implication on Spectral Properties and Parental Bodies. *Icarus* 371: 114653. https://doi.org/10.1016/j.icarus.2021.114653.

Carli, C., Pratesi, G., Moggi-Cecchi, V., Zambon, F., Capaccioni, F., and Santoro, S. 2018. Northwest Africa 6232: Visible-Near Infrared Reflectance Spectra Variability of an Olivine Diogenite. *Meteoritics & Planetary Science* 53: 2228–42.

Clark, R. N. 1999. Chapter 1: Spectroscopy of Rocks and Minerals, and Principles of Spectroscopy. In *Manual of Remote Sensing*, edited by A. Z. Rencz, 3–58. New York, NY: Wiley & Sons Press.

Clark, R. N., and Roush, T. L. 1984. Reflectance Spectroscopy: Quantitative Analysis Techniques for Remote Sensing Applications. *Journal of Geophysical Research* 89: 6329–40.

Cloutis, E. A., Gaffey, M. J., Jackowski, T. L., and Reed, K. L. 1986. Calibrations of Phase Abundance, Composition, and Particle Size Distribution for Olivine-Orthopyroxene Mixtures from Reflectance Spectra. *Journal of Geophysical Research* 91(B11): 11641–53. https://doi.org/10.1029/JB091iB11p11641.

Cloutis, E. A., Hudon, P., Romanek, C. S., Bishop, J. L., Reddy, V., Gaffey, M. J., and Hardersen, P. S. 2010. Spectral Reflectance Properties of Ureilites. *Meteoritics & Planetary Science* 45: 1668–94.

Crossley, S. D., Ash, R. D., Sunshine, J. M., Corrigan, C. M., McCoy, T. J., Mittlefehldt, D. W., and Puchtel, I. S. 2020. Sulfide-Dominated Partial Melting Pathways in Brachinites. *Meteoritics & Planetary Science* 55: 2021–43.

Day, J. M. D., Ash, R. D., Liu, Y., Bellucci, J. J., Rumble, D., III, McDonough, W. F., Walker, R. J., and Taylor, L. 2009. Early Formation of Evolved Asteroidal Crust. *Nature* 457: 179–83.

Day, J. M. D., Corder, C. A., Assayag, N., and Cartigny, P. 2019. Ferrous Oxide-Rich Asteroid Achondrites. *Geochimica et Cosmochimica Acta* 266: 544–67.

19455100, 2023, 6, Downloaded from https://onlinelibrary.wiley.com/doi/10.1111/maps.13998 by Universita Di Firenze Sistema, Wiley Online Library on [10/08/2023]. See the Terms and Conditions (https://onlinelibrary.wiley.com/terms-and-conditions) on Wiley Online Library for rules of use; OA articles are governed by the applicable Creative Commons License

Day, J. M. D., Walker, R. J., Ash, R. D., Liu, Y., Rumble, D., III, Irving, A. J., Goodrich, C. A., Tait, K., McDonough, W. F., and Taylor, L. A. 2012. Origin of Felsic Achondrites Graves Nunataks 06128 and 06129, and Ultramafic Brachinites and Brachinite-Like Achondrites by Partial Melting of Volatile-Rich Primitive Parent Bodies. *Geochimica et Cosmochimica Acta* 81: 94–128.

De Leon, J., Licandro, J., Duffard, R., and Serra-Ricart, M. 2006. Spectral Analysis and Mineralogical Characterization of 11 Olivine–Pyroxene Rich NEAs. *Advances in Space Research* 37: 178–83. https://doi.org/10.1016/j.asr.2005.05.074.

Delaney, J. S., Zanda, B., Clayton, R. N., and Mayeda, T. 2000. Zg(b): A Ferroan Achondrite Intermediate Between Brachinites and Londranites. 31st Lunar and Planetary Science Conference, abstract #1745.

DeMeo, F. E., Burt, B. J., Marsset, M., Polishook, D., Burbine, T. H., Carry, B., Binzel, R. P., et al. 2022. Connecting Asteroids and Meteorites with Visible and Near-Infrared Spectroscopy. *Icarus* 380: 114971. https://doi.org/10.1016/j.icarus.2022.114971.

Domeneghetti, M. C., Fioretti, A. M., Cámara, F., McCammon, C., and Alvaro, M. 2013. Thermal History of Nakhlites: A Comparison between MIL 03346 and its Terrestrial Analogue Theo's Flow. *Geochimica et Cosmochimica Acta* 121: 571–81.

Fabriès, J. 1979. Spinel-Olivine Geothermometry in Peridotites from Ultramafic Complexes. *Contributions to Mineralogy and Petrology* 69: 329–36.

Feldstein, S. N., Jones, R. H., and Papike, J. J. 2001. Disequilibrium Partial Melting Experiments of the Leedey L6 Chondrite: Textural Controls on Melting Processes. *Meteoritics & Planetary Science* 36: 1421–41.

Floss, C. 2000. Complexities on the Acapulcoite-Lodranite Parent Body: Evidence from Trace Element Distributions in Silicate Minerals. *Meteoritics & Planetary Science* 35: 1073–85.

Floss, C., Crozaz, G., Jolliff, B., Benedix, G., and Colton, S. 2008. Evolution of the Winonaite Parent Body: Clues from Silicate Mineral Trace Element Distributions. *Meteoritics & Planetary Science* 43: 657–74.

Floss, C., Jolliff, B., Benedix, G., Stadermann, F. J., and Reid, J. 2007. Hammadah al Hamra 193: The First Amphibole-Bearing Winonaite. *American Mineralogist* 92: 460–7.

Gaffey, M. J., Bell, J. F., Brown, R. H., Burbine, T. H., Piatek, J. L., Reed, K. L., and Chaky, D. A. 1993. Mineralogical Variations Within the S-Type Asteroid Class. *Icarus* 106: 573–602. https://doi.org/10.1006/icar.1993.1194.

Gardner-Vandy, K. G., Lauretta, D. S., and McCoy, T. J. 2013. A Petrologic, Thermodynamic and Experimental Study of Brachinites: Partial Melt Residues of an R Chondrite-Like Precursor. *Geochimica et Cosmochimica Acta* 122: 36–57.

Goodrich, C. A. 1992. Ureilites: A Critical Review. *Meteoritics* 27: 327–52.

Goodrich, C. A., Kita, N. T., Spicuzza, M. J., Valley, J. W., Zipfel, J., Mikouchi, T., and Miyamoto, M. 2011. The Northwest Africa 1500 Meteorite: Not a Ureilite, Maybe a Brachinite. *Meteoritics & Planetary Science* 45: 1906–28.

Goodrich, C. A., Kita, N. T., Sutton, S. R., Wirick, S., and Gross, J. 2017. The Miller Range 090340 and 090206 Meteorites: Identification of New Brachinite-Like Achondrites with Implications for the Diversity and Petrogenesis of the Brachinite Clan. *Meteoritics & Planetary Science* 52: 949–78.

Grady, M., Pratesi, G., and Moggi, C. V. 2014. *Atlas of Meteorites*. Cambridge: Cambridge University Press. 384.

Greenwood, R. C., Burbine, T. H., Miller, M. F., and Franchi, I. A. 2017. Melting and Differentiation of Early-Formed Asteroids: The Perspective from High Precision Oxygen Isotope Studies. *Chemie der Erde* 77: 1–43.

Greenwood, R. C., Franchi, I. A., Gibson, J. M., and Benedix, G. K. 2007. Oxygen Isotope Composition of the Primitive Achondrites. 38th Lunar and Planetary Science Conference, abstract #2163.

Greenwood, R. C., Franchi, I. A., Gibson, J. M., and Benedix, G. K. 2012. Oxygen Isotope Variation in Primitive Achondrites: The Influence of Primordial, Asteroidal and Terrestrial Processes. *Geochimica et Cosmochimica Acta* 94: 146–63.

Grossman, J. N. 1998. *Meteoritical Bulletin*, No. 82. *Meteoritics & Planetary Sciences* 33: A221–39.

Hasegawa, H., Mikouchi, T., Yamaguchi, A., Yasutake, M., Greenwood, R. C., and Franchi, I. A. 2019. Petrological, Petrofabric, and Oxygen Isotopic Study of Five Ungrouped Meteorites Related to Brachinites. *Meteoritics & Planetary Science* 54: 1–16. https://doi.org/10.1111/maps.13249.

Hiroi, T., Bell, J. F., Takeda, H., and Pieters, C. M. 1993. Modeling of S-Type Asteroid Spectra Using Primitive Achondrites and Iron Meteorites. *Icarus* 102: 107–16. https://doi.org/10.1006/icar.1993.1036.

Irving, A. J., Kuehner, S. M., and Ziegler, K. 2013. Petrology and Oxygen Isotopic Composition of Brachinite-Like Achondrites Northwest Africa 7388 and Northwest Africa 7605, and Evidence for Late-Stage Methane-Triggered Reduction. 44th Lunar and Planetary Science Conference, abstract #2192.

Johnson, J. E., Scrymgour, J. M., Jarosewich, E., and Mason, B. 1977. Brachina Meteorite: A Chassignite from South Australia. *Records of the South Australian Museum* 17: 309–19.

Johnson, C. A., and Prinz, M. 1991. Chromite and Olivine in Type II Chondrules in Carbonaceous and Ordinary Chondrites: Implications for Thermal Histories and Group Differences. *Geochimica et Cosmochimica Acta* 55: 893–904.

Keil, K. 2014. Brachinite Meteorites: Partial Melt Residues from an FeO-Rich Asteroid. *Chemie der Erde/Geochemistry* 74: 311–29.

Kessel, R., Beckett, J. R., and Stolper, E. M. 2007. The Thermal History of Equilibrated Ordinary Chondrites and the Relationship Between Textural Maturity and Temperature. *Geochimica et Cosmochimica Acta* 71: 1855–81.

Kiddel, C. B., Cloutis, E. A., Dagdick, B. R., Stromberg, J. M., Applin, D. M., and Mann, J. P. 2018. Spectral Reflectance of Powder Coating on Carbonaceous Chondrite Slabs. Implications for Asteroid Regolith Observations. *Journal of Geophysical Research: Planets* 123: 2803–40.

Lucas, M. P., Emery, J. P., Hiroi, T., and McSween, Y. 2019. Spectral Properties and Mineral Compositions of Acapulcoite-Lodranite Clan Meteorites: Establishing S-Type Asteroid-Meteorite Connections. *Meteoritics & Planetary Science* 54: 157–80. https://doi.org/10.1111/maps.13203.

19455100, 2023, 6, Downloaded from https://onlinelibrary.wiley.com/doi/10.1111/maps.13998 by Universita Di Firenze Sistema, Wiley Online Library on [10/08/2023]. See the Terms and Conditions (https://onlinelibrary.wiley.com/terms-and-conditions) on Wiley Online Library for rules of use; OA articles are governed by the applicable Creative Commons License

Mittlefehldt, D. W. 2014. Achondrites. In *Meteorites, Comets, and Planets. Treatise on Geochemistry*, edited by H. D. Holland, and K. K. Turekian, vol. 1, 235–66. Oxford: Elsevier Pergamon.

Mittlefehldt, D. W., Bogard, D. D., Berkley, J. L., and Garrison, D. H. 2003. Brachinites: Igneous Rocks from a Differentiated Asteroid. *Meteoritics & Planetary Science* 38: 1601–25.

Mittlefehldt, D. W., McCoy, T. J., Goodrich, C. A., and Kracher, A. 1998. Non-chondritic Meteorites from Asteroidal Bodies. In *Planetary Materials*. Reviews in Mineralogy, edited by J. J. Papike, vol. 36, 195. Washington, DC: Mineralogical Society of America.

Murri, M., Cámara, F., Adam, J., Domeneghetti, M. C., and Alvaro, M. 2018. Intracrystalline "Geothermometry" Assessed on Clino and Orthopyroxene Bearing Synthetic Rocks. *Geochimica et Cosmochimica Acta* 227: 133–42.

Murri, M., Domeneghetti, M. C., Fioretti, A. M., Nestola, F., Vetere, F., Perugini, D., Pisello, A., Faccenda, M., and Alvaro, M. 2019. Cooling History and Emplacement of a Pyroxenitic Lava as Proxy for Understanding Martian Lava Flows. *Science Reports* 9: 1–7.

Murri, M., Scandolo, L., Fioretti, A. M., Nestola, F., Domeneghetti, C. M., and Alvaro, M. 2016. The Role of Fe Content on the Fe-Mg Exchange Reaction in Augite. *American Mineralogist* 101: 2747–50.

Nehru, C. E., Prinz, M., Delaney, J. S., Dreibus, G., Palme, H., Spettel, B., and Wänke, H. 1983. Brachina: A New Type of Meteorite, not a Chassignite. Proceedings, 14th Lunar and Planetary Science Conference. *Journal of Geophysical Research* 88: B237–44.

Petaev, M. I., and Brearley, A. J. 1994. Exsolution in Ferromagnesian Olivine of the Divnoe Meteorite. *Science* 266: 1545–7. https://doi.org/10.1126/science.266.5190.1545.

Pieters, C. M., and Hiroi, T. 2004. RELAB (Reflectance Experiment Laboratory): A NASA Multiuser Spectroscopy Facility. 35th Lunar and Planetary Science Conference, abstract #1720.

Rumble, D., III, Irving, A. J., Bunch, T. E., Wittke, J. H., and Kuehner, S. M. 2008. Oxygen Isotopic and Petrological Diversity Among Brachinites NWA 4872, NWA 4874, NWA 4882, and NWA 4969: How Many Ancient Parent Bodies? 39th Lunar and Planetary Science Conference, abstract #1974.

Ruzicka, A., Grossman, J., Bouvier, A., Herd, C. D. K., and Agee, C. B. 2015. *Meteoritical Bulletin*, No. 101. *Meteoritics & Planetary Sciences* 50: 166.

Sack, R. O., and Ghiorso, M. S. 1989. Importance of Considerations of Mixing Properties in Establishing an Internally Consistent Database: Thermochemistry of Minerals in the System Mg_2SiO_4-Fe_2SiO_4-SiO_2. *Contributions to Mineralogy and Petrology* 102: 41–68.

Sack, R. O., and Ghiorso, M. S. 1991a. Chromian Spinels as Petrogenetic Indicators: Thermodynamics and Petrological Applications. *American Mineralogist* 76: 827–47.

Sack, R. O., and Ghiorso, M. S. 1991b. An Internally Consistent Model for the Thermodynamic Properties of Fe-Mg-Titanomagnetite-Aluminate Spinels. *Contributions to Mineralogy and Petrology* 106: 474–505.

Sack, R. O., and Ghiorso, M. S. 1994a. Thermodynamics of Multicomponent Pyroxenes: III. Calibration of Fe^{2+}(Mg)-1, TiAl(MgSi)-1, $TiFe^{3+}$(MgSi)-1, $AlFe^{3+}$(MgSi)-1, NaAl (CaMg)-1, Al_2(MgSi)-1 and Ca(Mg)-1 Exchange Reactions Between Pyroxenes and Silicate Melts. *Contributions to Mineralogy and Petrology* 118: 271–96.

Sack, R. O., and Ghiorso, M. S. 1994b. Thermodynamics of Multicomponent Pyroxenes: I Formulation of a General Model. *Contributions to Mineralogy and Petrology* 116: 277–86.

Sack, R. O., and Ghiorso, M. S. 1994c. Thermodynamics of Multicomponent Pyroxenes: II Phase relations in the Quadrilateral. *Contributions to Mineralogy and Petrology* 116: 287–300.

Shearer, C. K., Burger, P. V., Neal, C., Sharp, Z., Spivak-Birndorf, L., Borg, L., Fernanded, V. A., et al. 2010. Non-basaltic Asteroidal Magmatism during the Earliest Stages of Solar System Evolution: A View from Antarctic Achondrites GravesNunatak 06128 and 06129. *Geochimica et Cosmochimica Acta* 74: 1172–99.

Takeda, H., Mori, H., and Ogata, H. 1989. Mineralogy of Augite-Bearing Ureilites and the Origin of Their Chemical Trends. *Meteoritics & Planetary Science* 24: 73–81. https://doi.org/10.1111/j.1945-5100.1989.tb00947.x.

Warren, P. H., and Kallemeyn, G. W. 1989. Allan Hills 84025: The Second Brachinite, Far More Differentiated than Brachina, and an Ultramafic Achondritic Clast from L Chondrite Yamato-75097. Proceedings of the 19th Lunar and Planetary Science Conference, pp. 475–86.

Weisberg, M. K., Smith, C., Benedix, G., Herd, C. D. K., Righter, K., Haack, H., Yamaguchi, A., Chennaoui, A. H., and Grossman, J. N. 2009. *Meteoritical Bulletin*, No. 96. *Meteoritics & Planetary Sciences* 44: 1355–97.

Wlotzka, F. 1972. Havero Ureilite: Evidence for Recrystallization and Partial Reduction. *Meteoritics* 7: 591–600.

Wlotzka, F. 1985. Olivine-Spinel and Olivine-Ilmenite Thermometry in Chondrites of Different Petrologic Type. 16th Lunar and Planetary Science Conference. Abstract #1469. pp. 918–9.

Wlotzka, F. 2005. Cr Spinel and Chromite as Petrogenetic Indicators in Ordinary Chondrites: Equilibration Temperatures of Petrologic Types 3.7 to 6. *Meteoritics & Planetary Science* 40: 1673–702.

Zema, M., Domeneghetti, M. C., Molin, G. M., and Tazzoli, V. 1997. Cooling Rates of Diogenites: A Study of Fe^{2+}-Mg Ordering in Orthopyroxene by Single-Crystal X-Ray Diffraction. *Meteoritics & Planetary Science* 32: 855–62.

Zolensky, M. E., Herrin, J., Mikouchi, T., Ohsumi, K., Friedrich, J., Steele, A., Fries, M., et al. 2010. Mineralogy and Petrography of the Almahata Sitta Ureilite. *Meteoritics & Planetary Science* 45: 1812–20. https://doi.org/10.1111/j.1945-5100.2010.01111.x.

SUPPORTING INFORMATION

Additional supporting information may be found in the online version of this article.

Data S1. Reflectance spectra of Al Huwaysah 010.

Data S2. Supplementary Methods, Figures and Tables.

19455100, 2023, 6, Downloaded from https://onlinelibrary.wiley.com/doi/10.1111/maps.13998 by Universita Di Firenze Sistema, Wiley Online Library on [10/08/2023]. See the Terms and Conditions (https://onlinelibrary.wiley.com/terms-and-conditions) on Wiley Online Library for rules of use; OA articles are governed by the applicable Creative Commons License